Potential-Dependent Studies on the Interaction between Phenylalanine-Substituted Bombesin Fragments and Roughened Ag, Au, and Cu Electrode Surfaces

Edyta Podstawka,*,† Gediminas Niaura,‡ and Leonard M. Proniewicz†

Faculty of Chemistry, Jagiellonian University, ul. Ingardena 3, 30-060 Krakow, Poland, and Department of Bioelectrochemistry and Biospectroscopy, Institute of Biochemistry, Mokslininkų 12, LT-08662 Vilnius, Lithuania

Received: September 26, 2009; Revised Manuscript Received: November 11, 2009

In this work, we report systematic surface-enhanced Raman spectroscopy (SERS) and generalized two-dimensional correlation analysis (G2DCA) studies of the structures of five specifically modified phenylalanine-substituted C-terminal bombesin 6−14 fragments (BN^{6-14}). The fragments studied have all been tested as chemotherapeutic agents in cancer therapy, and they form amino acid sequences in bombesin: cyclo[D-Phe^6,His^7,Leu^{14}]BN^{6-14}, [D-Phe^6,Leu-$NHEt^{13}$,des-Met^{14}]BN^{6-14}, [D-Phe^6,Leu^{13}-(Ⓡ)-p-Cl-Phe^{14}]BN^{6-14}, [D-Phe^6,β-Ala^{11},Phe^{13},Nle^{14}]BN^{6-14}, and [D-Tyr^6,β-Ala^{11},Phe^{13},Nle^{14}]BN^{6-14}. We adsorbed these fragments onto roughened Ag, Au, and Cu electrode surfaces, using a potential range from −1.200 to 0.400 V, at physiological pH. We compared the adsorption mechanism of each fragment on these substrates, as well any changes observed with varying electrode potential, to determine the relationship between adsorption strength and geometry of each of the peptides wherever it was possible. For example, we showed that none of these fragments directly interact with the Ag, Au, and Cu surfaces via residues of Phe (phenylalanine) and Trp^8 (L-tryptophane at position 8 of the BN amino acid sequence) or by an amide bond, due to a very small shift in wavenumber of their characteristic vibrations. Specific interactions were recognized from the broadening, wavenumber shift, and increase in intensity of the W18 Trp^8 mode near 759 cm^{-1} and decrease in ν_{12} vibration frequency of the Phe residue. In general, more intense SERS bands were observed due to the Phe ring, compared with the Trp^8 ring, which suggested a preferential adsorption of phenylalanine over tryptophane. For [D-Tyr^6,β-Ala^{11},Phe^{13},Nle^{14}]BN^{6-14}, the data also suggest some interaction of a D-Tyr^6 residue (D-tyrosine at position 6). Finally, only slight rearrangements of these moieties on the substrates are observed with changes in electrode potential.

Introduction

Brain, gastric, pancreatic, prostate, breast, colon, and pulmonary tumors are the most frequently diagnosed malignancies in humans. Endogenous neurotransmitters like bombesin (BN, pGlu-Gln-Arg-Leu-Gly-Asn-Gln-Trp-Ala-Val-Gly-His-Leu-Met-NH_2, where pGlu is 5-oxo-proline) have been widely recognized as important growth factors involved in carcinogenesis and the progression of these diseases.[1−6] Understanding even pieces of the molecular basis of the development of these diseases is a critical step toward their diagnosis and possible treatment. Unfortunately, at present, the mechanism by which BN stimulates tumor growth still remains unclear. One way to resolve this problem is to study the large existing number of specifically modified BN analogues and fragments. This is also an efficient approach to designing novel chemotherapeutic drugs and diagnostic agents.

In this regard, several series of G-protein-coupled receptor antagonists have been developed and tested. These have illuminated some important structural components that might contribute to the unique ability of these peptides to interact with rGRP-R (bombesin/GRP-preferring subtype receptor) with high affinity.[7−20] These peptides include BN analogues and fragments resulting from side chain modification strategies (amino acid deletions or the retro-inverso modification); peptides with modified peptide bonds; peptides with a modified or deleted C-terminal region; and bombesin-related peptides. It has been demonstrated, for example, that the C-terminal nanopeptide (BN^{6-14}) is the minimal fragment required for full BN affinity.[21,22] It has also been determined that deletion or substitution of the L-tryptophan residue in position 8 of the BN amino acid sequence (Trp^8) produces an inactive analogue. Hence, Trp^8 is believed to be responsible for receptor recognition.[23] Furthermore, it has been shown that steric requirements for the aromatic amino acid substituted at position 6 of BN do not appear to be very exacting, as only a slight decrease in potency (<3-fold) was detected between D-Trp^6, D-Tyr^6 (D-tyrosine), and D-Phe^6 (D-phenylalanine) derivatives. Finally, the addition of an electron-withdrawing group to the aromatic moiety (D-*p*-chlorophenylalanine, D-*p*-Cl-Phe) also has only a minimal effect on potency.[24]

The polar Gln^7 residue (L-glutamine at position 7) plays a key role in recognizing the receptor pathway in mammalian pancreatic acinar cells. In addition, Asp^{87} (L-asparagine), a negatively charged amino acid in the second hydrophobic transmembrane domain of rGRP-R, may preferentially form an ionic bond with a positively charged amino acid such as His^7 (L-histidine at position 7), producing an increase in rGRP-R affinity.[25] Moreover, it has been shown that the C-terminal Met (L-methionine) side chain is not essential for BN agonist activity, since other diverse amino acid substitutions in position 14, i.e., norleucine (Nle^{14}), also yield agonists.[24,26,27] However, it is apparent that the carboxamide group at this position is of prime

* To whom correspondence should be addressed. E-mail: podstawk@chemia.uj.edu.pl. Phone: +48-12-663-2077. Fax: +48-12-634-0515.
† Jagiellonian University.
‡ Institute of Biochemistry.

10.1021/jp909268c
Published on Web 12/21/2009

importance in the biological activity of BN, since its removal always produces pure antagonists.[24,28] It is also unlikely that Phe^{13} is a major factor in the high affinity for rGRP-R. However, the presence of a penultimate phenylalanine could play an important role in combination with alterations in other locations; in general, the peptides with this substitution had a higher affinity for the hBRS-3 (the orphan subtype-3 receptor) than those with an L-leucine (Leu) at this position.[29]

It has also been suggested that another important substitution is that of β-alanine at position 11 (β-Ala^{11}) of BN.[30] However, it remains unclear whether the principal effect of this substitution is only an extension of the length of the peptide backbone or whether there are other factors, such as side chain modification.[30] Importantly, substitution of D-Ala^{11} (D-alanine at position 11) tends to stabilize the required BN folding without compromising activity.[7] Alkyl substituents at position 13 of the NH_2 group dramatically improve binding affinity and antagonist potency. This perhaps implies that the CO at position 13 is involved in binding to the bombesin/rGRP-R complex via hydrogen bonding, since such an interaction would be enhanced by electron-releasing alkyl substituents.[28] Recently, a number of research efforts have been focused on a synthetic analogue of BN, [D-Tyr^6,β-Ala^{11},Phe^{13},Nle^{14}]BN^{6-14}, which functions as a universal ligand with high affinity to each of three mammalian receptors, a unique and important property since different cancers may possess different BN receptor classes.

The brief introduction presented above focused its attention on the conformations of differently modified analogues and their possible roles in interaction with receptors. A complementary approach is to use a surface-enhanced Raman scattering (SERS) technique that makes it possible to obtain further insight into the different types of supramolecular architecture of BN and its analogues and into their adsorption phenomena at the peptide level.[31−40] However, it has to be made perfectly clear that this study may allow the most active amino acids that are involved in the adsorption mechanism to be traced; however, they cannot mimic the substrate−receptor system. On the other hand, there are a few coinciding structure/function (activity) facts between SERS results and those obtained from biochemical data, which will be discussed further in the paper.

Motivated by the biological importance of BN and the possibility of understanding the adsorption mechanism at the solid/solution interface, we performed a number of spectroscopic studies on it and its specifically modified fragments. Previously, we determined the adsorbed molecular structures of BN and bombesin-like peptides on both an electrochemically roughened Ag electrode surface and an Ag colloidal sol using SERS.[33−36] We studied the adsorption mechanism on these surfaces, and observed changes in the adsorption process by substituting natural amino acids with synthetic amino acids. We studied six modified BN analogues, including [D-Phe^{12}]BN, [Tyr^4]BN, [Tyr^4,D-Phe^{12}]BN, [D-Phe^{12},Leu^{14}]BN, [Leu^{13}-(Ⓡ)-Leu^{14}]BN, and [Lys^3]BN.[33,34]

Recently, we have also conducted SERS characterization of seven 6−14 fragments of the bombesin amino acid sequence adsorbed at Ag substrates, including cyclo[D-Phe^6,His^7,Leu^{14}]-BN^{6-14}, [D-Phe^6,Leu-$NHEt^{13}$,des-Met^{14}]BN^{6-14}, [D-Phe^6,Leu^{13}-(Ⓡ)-p-Cl-Phe^{14}]BN^{6-14}, [D-Phe^6,β-Ala^{11},Phe^{13},Nle^{14}]BN^{6-14}, [D-Tyr^6,β-Ala^{11},Phe^{13},Nle^{14}]BN^{6-14}, [D-Tyr^6,β-Phe^{11},Phe^{13},Nle^{14}OH]BN^{6-14}, and [D-Cys^6,Asn^7,D-Ala^{11},Cys^{14}]BN^{6-14}.[37,38] For these fragments, we correlated the relative potency of inhibition of ^{125}I-[Tyr^4]BN binding to rat pancreas acini cells with the behavior of the amide bond on the Ag substrates. We tried to also correlate the SERS patterns with the contribution of each structural component to the ability to interact with rGRP-R, showing that these amino acids that are the most active in adsorption mechanism at the silver surface show also very high affinity to the rGRP-R (however, it does not mean that we assume that the silver surface can mimic a structure of the receptor). On the other hand, there are few strong, surprising coincidences that are pointed out briefly below. For example, we showed that the first five amino acids of the BN N-terminus do not influence the adsorption mechanism on Ag surfaces, and likewise they are not essential for interaction with rGRP-R.[24] In addition, based on the almost exclusive enhancement of the Trp^8 bands in the SERS spectra of BN, its modified analogues and fragments, and related peptides, we concluded that Trp^8 is responsible for binding to the Ag substrates, and that it is also responsible for receptor recognition.[23]

The strong enhancement of the C═O vibrations for BN and its analogues and fragments, except for [Leu^{13}-Ⓡ-Leu^{14}]BN and [D-Phe^6,Leu^{13}-Ⓡ-p-Cl-Phe^{14}]BN^{6-14}, confirmed the key role of the C═O fragment in recognizing the receptor pathway in pancreatic acinar cells.[28] Deletion of Met^{14} ([D-Phe^6,Leu-$NHEt^{13}$,des-Met^{14}]BN^{6-14}) or substitution of Met^{14} with Leu^{14}, Phe^{14}, or Nle^{14} ([D-Phe^{12},Leu^{14}]BN, [D-Phe^6,Leu^{13}-(Ⓡ)-p-Cl-Phe^{14}]BN^{6-14}, [D-Phe^6,β-Ala^{11},Phe^{13},Nle^{14}]BN^{6-14}, [D-Tyr^6, β-Ala^{11},Phe^{13},Nle^{14}]BN^{6-14}, [D-Tyr^6,β-Phe^{11},Phe^{13},Nle^{14}OH]BN^{6-14}, and [D-Cys^6,Asn^7,D-Ala^{11},Cys^{14}]BN^{6-14}, respectively) does not change the general adsorption mechanism of these peptides through the Trp^8 residue, C═O fragment, or amide bond, except in [Leu^{13}-(Ⓡ)-Leu^{14}]BN and [D-Phe^6, Leu^{13}-(Ⓡ)-p-Cl-Phe^{14}]BN^{6-14}. This is in agreement with biological activity studies showing that such modifications are not particularly important in the expression of biological activity at rGRP-R.[25]

Additionally, the observed SERS signals for carboxy-terminated fragments of bombesin of various lengths (X-14 of the amino acid sequence, i.e., BN^{13-14}, BN^{12-14}, BN^{11-14}, BN^{10-14}, BN^{9-14}, and BN^{8-14}) in Ag colloidal solutions were compared with the contribution of the structural components of t hese fragments to their possible structures formed at the interface.[39] Most recently, we characterized potential-dependent changes in the orientation of BN on electrochemically roughened Ag, Au, and Cu electrode surfaces at physiological pH.[40] In addition, to amplify slight changes among the spectra at different applied Ag, Au, or Cu electrode potentials, we applied generalized two-dimensional correlation analysis (G2DCA).

All of these investigations, together with biological activity studies, have shown that an electrochemically roughened Ag electrode surface is a more selective substrate than a colloidal Ag surface. Further changes in selectivity might be triggered by the electrode potential and by the nature of the electrode itself. Because biological recognition usually takes place at a charged interface, experiments at controlled potential make it possible to elucidate specific electric field-induced effects. Therefore, our present work focuses on analysis with roughened electrode surfaces of Ag, Au, and Cu. To further understand the physiological function of BN and its binding affinity, we aimed to investigate the effect of Phe substitution in the five 6−14 fragments of BN, i.e., in cyclo[D-Phe^6,His^7,Leu^{14}]BN^{6-14}, [D-Phe^6,Leu-$NHEt^{13}$,des-Met^{14}] BN^{6-14}, [D-Phe^6,Leu^{13}-(Ⓡ)-p-Cl-Phe^{14}]BN^{6-14}, [D-Phe^6,β-Ala^{11},Phe^{13},Nle^{14}]BN^{6-14}, and [D-Tyr^6,β-Ala^{11},Phe^{13},Nle^{14}]BN^{6-14}. We studied the adsorption mechanisms of these fragments on roughened Ag, Au, and Cu electrode surfaces at different applied electrode potentials. In order to better understand these results, we characterized changes in the SERS band enhancement, broadness, and wavenumber arising from the constituents' amino acids, as well as from the

functional groups of the adsorbed species, as a function of the type of metal substrate and the applied electrode potential. The SERS spectral signals change as a function of electrode potential due to slight alterations in the molecular geometry of the substrate. In this way, we provide missing structural information concerning the chemisorption of BN and its Phe-substituted BN^{6-14} fragments on the roughened metal electrode surface. Generalized two-dimensional correlation spectroscopy, which emphasizes spectral features not readily observed in conventional one-dimensional spectra, was additionally applied for a detailed analysis of the SERS spectral signals.

As discussed in the paper, due to the nature of the adsorbate geometry, adsorption phenomena provide a unique and unprecedented method of probing a protein/surface interface at the molecular level and obtaining specific information about molecular conformational changes occurring at this interface.[41] This is because, at the interface between the biomolecule and metal surface, peptides have regions that directly interact with this surface. The amino acid composition and the sequence of these contact regions usually determine the adsorption behavior of peptides onto particular metal surfaces. Therefore, analysis of the SERS signal (enhancement, broadness, and wavenumber) coming from constituents' amino acids is useful for understanding possible ways in which a peptide interacts with its surrounding medium, and, by extension, how a substrate binds to the solid/solution interface.[31−40] These interactions are believed to be of great significance for the understanding of the *in vivo* behavior of implants. Therefore, there is strong motivation to develop simple and rapid *in vitro* or, if possible, *in vivo* methods (biosensors) for studying adsorption phenomena at the protein level. The surface-enhanced Raman scattering (SERS) technique is believed to be one of them.

Experimental Section

Neurotransmitters. 6−14 fragments of bombesin (BN^{6-14}) amino acid sequence, substituted by phenylalanine (Phe) at the positions 6, 13, and 14, were purchased from Bachem Co. (Switzerland) and Phoenix Pharmaceuticals Inc. (USA). These fragments included cyclo[D-Phe^6,His^7,Leu^{14}]BN^{6-14}, [D-Phe^6,Leu-$NHEt^{13}$,des-Met^{14}]BN^{6-14}, [D-Phe^6,Leu^{13}-(Ⓡ)-p-Cl-Phe^{14}]BN^{6-14}, [D-Phe^6,β-Ala^{11},Phe^{13},Nle^{14}]BN^{6-14}, and [D-Tyr^6,β-Ala^{11},Phe^{13},Nle^{14}]BN^{6-14}. Their purity and chemical structure were determined using ^1H and ^{13}C NMR spectra (Bruker Avance DRX 300 MHz spectrometer) and electrospray mass spectrometry (Finnigan Mat TSQ 700).

SERS Measurements. Near-infrared SERS spectra were recorded using an Echelle type RamanFlex 400 spectrometer (PerkinElmer, Inc.) equipped with a thermoelectrically cooled (−50 °C) CCD camera and fiber-optic cable for excitation and collection of the Raman spectra. The 785 nm beam of the diode laser was used as the excitation source, and the sample was set in a 180° scattering geometry. The laser power at the sample was restricted to 50 mW, and the beam was focused to a 200 μm diameter spot on the electrode with an integration time of 10 s. Each spectrum was recorded with an accumulation of 30 scans. Spectro-electrochemical measurements were carried out in a cylindrical three-electrode moving cell. The working electrode was a flat circle, approximately 5 mm in diameter, of Ag, Au, or Cu press-fitted into a Teflon rod. Platinum wire was the counter electrode, and the reference electrode was KCl saturated Ag/AgCl. All potential values in this work are reported relative to this reference electrode. During the experiment, ultrapure Ar gas was continuously bubbled through the solution to remove dissolved oxygen. The working electrode was placed approximately 3 mm from the cell window. In order to reduce thermal and light-induced effects, the cell and the electrodes were moved linearly with respect to the laser beam at a rate of about 15−25 mm/s.[42,43] Raman frequencies were calibrated using the polystyrene standard (ASTM E 1840) spectrum. Intensities were calibrated by a NIST intensity standard (SRM 2241). Experiments were conducted at 20 °C.

The Au electrode for SERS was electrochemically roughened by potential scanning for 50 cycles in a 0.1 M aqueous KCl solution between −0.30 and 1.31 V at a scan rate of 300 mV, as previously reported.[44,45] Electrochemical roughening procedures for the Ag and Cu electrodes were performed by established methods as described in refs 46 and 47, respectively.

Generalized Two-Dimensional Correlation Analysis. Generalized 2DC analysis of the SERS spectra of BN adsorbed on the roughened Ag, Au, and Cu electrode surfaces was performed using 2Dshige version 1.3 software, which was written by Shigeaki Morita, Kwansei-Gakuin University, 2004−2005. The four potential-dependent SERS spectra of BN were normalized. In the 2D-correlation maps, regions colored by red indicate positive correlation intensities, while blue regions indicate negative correlation intensities.

Results and Discussion

Structurally, cyclo[D-Phe^6,His^7,Leu^{14}]BN^{6-14}, [D-Phe^6,Leu-$NHEt^{13}$,des-Met^{14}]BN^{6-14}, [D-Phe^6,Leu^{13}-(Ⓡ)-p-Cl-Phe^{14}]BN^{6-14}, and [D-Phe^6,β-Ala^{11},Phe^{13},Nle^{14}]BN^{6-14} all have D-phenylalanine at position 6 of the BN amino acid sequence. [D-Phe^6,Leu^{13}-(Ⓡ)-p-Cl-Phe^{14}]BN^{6-14} and [D-Phe^6,β-Ala^{11}, Phe^{13},Nle^{14}]BN^{6-14} also contain D-Phe^6, and they possess p-Cl-Phe^{14} and Phe^{13} residues, respectively. Replacement of D-Phe^6 by D-Tyr^6 in [D-Phe^6,β-Ala^{11},Phe^{13},Nle^{14}]BN^{6-14} results in [D-Tyr^6,β-Ala^{11},Phe^{13},Nle^{14}]BN^{6-14}. Aside from natural amino acids, such as Trp^8 and His^{12} that have high affinity for a metal surface, the phenylalanine and D-tyrosine residues of these fragments are likely to be visible in the respective SERS spectra as long as they interact with the roughened Ag, Au, and Cu electrode surfaces in aqueous solution and at physiological pH.

Figures 1−5 compare the SERS spectra of these fragments taken with a diode laser at 785 nm. The spectra are those of cyclo[D-Phe^6,His^7,Leu^{14}]BN^{6-14}, [D-Phe^6,Leu-$NHEt^{13}$,des-Met^{14}]BN^{6-14}, [D-Phe^6,Leu^{13}-(Ⓡ)-p-Cl-Phe^{14}]BN^{6-14}, [D-Phe^6,β-Ala^{11},Phe^{13},Nle^{14}]BN^{6-14}, and [D-Tyr^6,β-Ala^{11},Phe^{13}, Nle^{14}]BN^{6-14} adsorbed on roughened Ag, Au, and Cu electrode surfaces at physiological pH in an electrode potential range from −1.200 to 0.400 V. As expected, these spectra almost exclusively possess the Raman bands characteristic of vibrations of Phe and Trp^8. In addition, low-intensity spectral features from the D-Tyr^6 residue, peptide bond, and methyl/methylene moiety are observed. The broad, intense bands near 550−580 and 940−960 cm^{-1} result from phosphate anions adsorbed at the Au and Cu electrodes, as does a rather weak spectral feature near 1109−1127 cm^{-1}.[48] Table 1 lists the wavenumbers of all the enhanced bands and their normal mode motions, using assignments based on previously determined results for BN and its analogues and fragments in Ag sol and on an electrode surface.[33,34,37,38,40] It also summarizes the spectral positions of these enhanced bands in the Raman spectra of these fragments in the solid state. Further information about normal mode assignments of the C-terminal BN^{11-14} fragment (Gly-His-Leu-Met-NH_2) was obtained from ref 39.

The most noteworthy point is that the SERS spectrum of every fragment investigated on the Ag, Au, and Cu electrodes at different electrode potentials resembles the SERS spectra of BN, its modified analogues, and fragments in Ag sol acquired

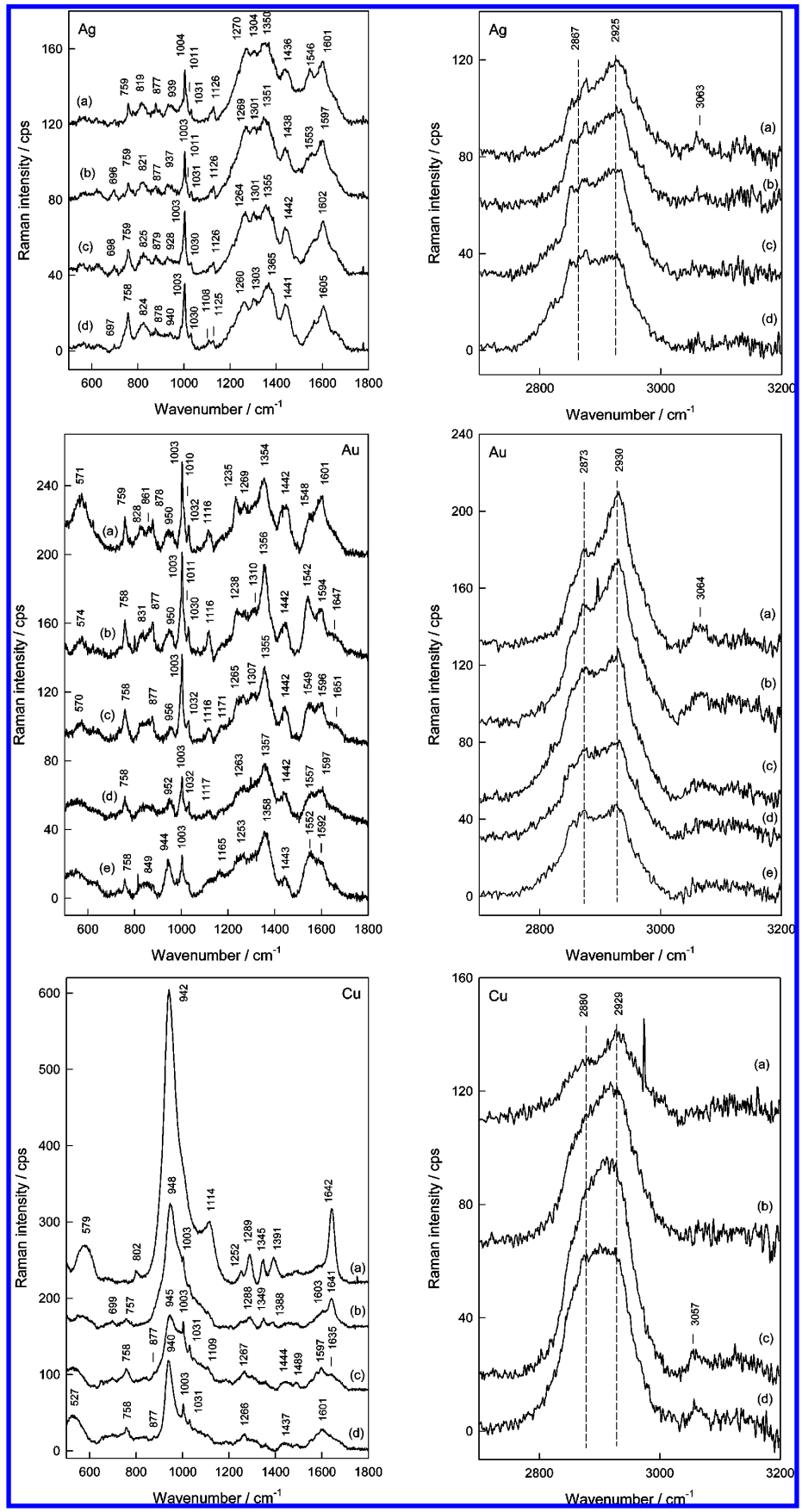

Figure 1. SERS spectra of cyclo[D-Phe^6,His^7,Leu^{14}]BN$^{6-14}$ adsorbed on roughened (A) Ag electrode at potentials of 0.000 V (a), −0.400 V (b), −0.800 V (c), and −1.200 V (d); (B) Au electrode at potentials of 0.400 V (a), 0.000 V (b), −0.400 V (c), −0.800 V (d), and −1.200 V (e); and (C) Cu electrode at potentials of −0.400 V (a), −0.800 V (b), −1.000 V (c), and −1.200 V (d). Measurement conditions are as follows: 0.1 M Na_2SO_4 solution containing 0.01 M phosphate buffer (pH 7.0) and 10^{-5} M peptide; excitation wavelength, 785 nm; laser power at the sample, 50 mW; integration time, 1500 s.

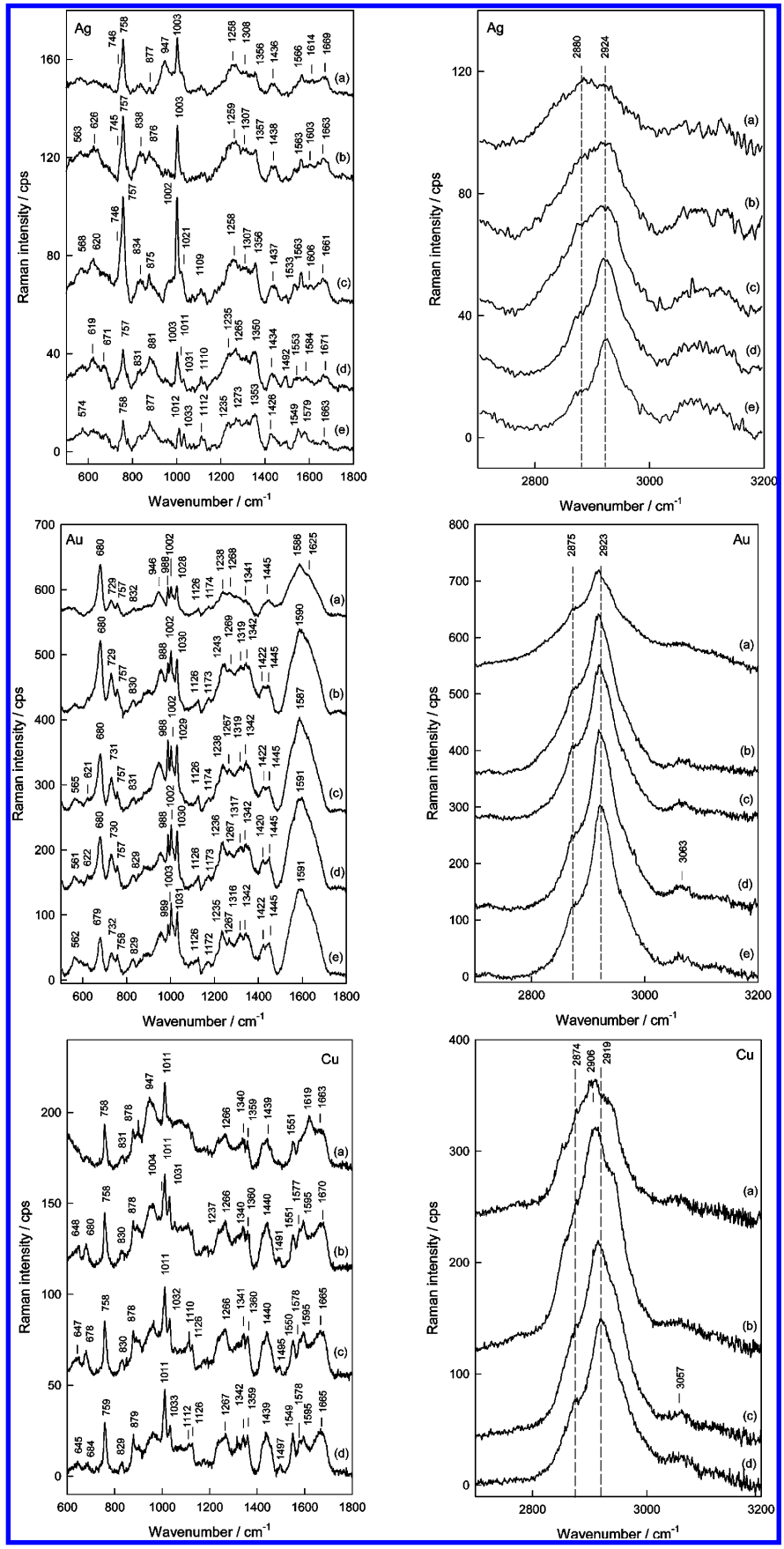

Figure 2. SERS spectra of [D-Phe^{6},Leu-NHEt^{13},des-Met^{14}]BN$^{6-14}$ adsorbed on roughened (A) Ag electrode at potentials of −1.200 V (a), −1.000 V (b), −0.800 V (c), −0.400 V (d), and 0.000 V (e); (B) Au electrode at potentials of −1.200 V (a), −0.800 V (b), −0.400 V (c), 0.000 V (d), and 0.400 V (e); and (C) Cu electrode at potentials of −1.200 V (a), −0.800 V (b), −0.600 V (c), and −0.200 V (d). Measurement conditions are as follows: 0.1 M Na_2SO_4 solution containing 0.01 M phosphate buffer (pH 7.0) and 10^{-5} M peptide; excitation wavelength, 785 nm; laser power at the sample, 50 mW; integration time, 1500 s.

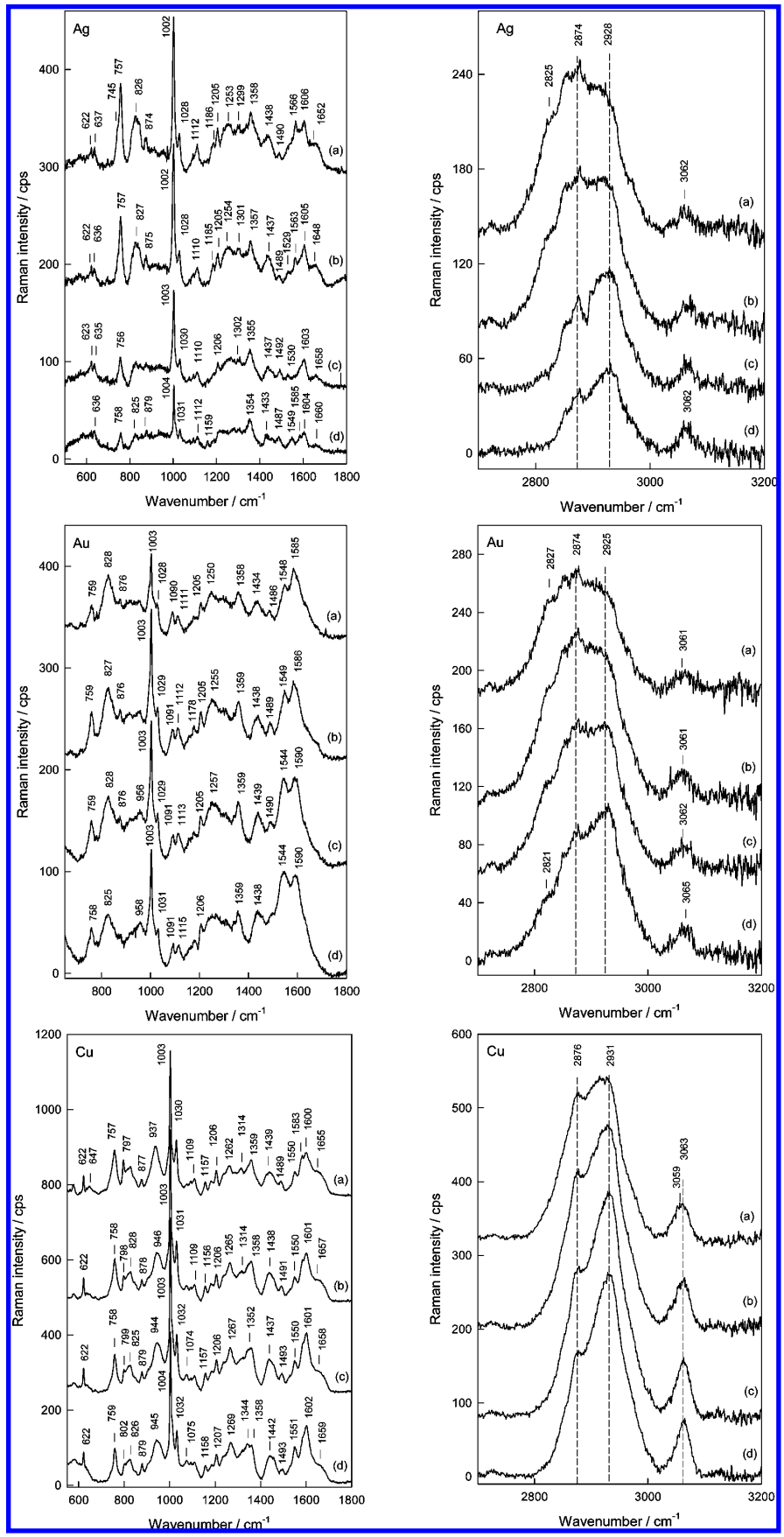

Figure 3. SERS spectra of [D-Phe^6,Leu^{13}-(Ⓡ)-p-Cl-Phe^{14}]BN$^{6-14}$ adsorbed on roughened (A) Ag electrode at potentials of −1.200 V (a), −0.800 V (b), −0.400 V (c), and 0.000 V (d); (B) Au electrode at potentials of −1.200 V (a), −0.800 V (b), −0.400 V (c), and 0.000 V (d); and (C) Cu electrode at potentials of −1.200 V (a), −0.800 V (b), −0.600 V (c), and −0.400 V (d). Measurement conditions are as follows: 0.1 M Na_2SO_4 solution containing 0.01 M phosphate buffer (pH 7.0) and 10^{-5} M peptide; excitation wavelength, 785 nm; laser power at the sample, 50 mW; integration time, 1500 s.

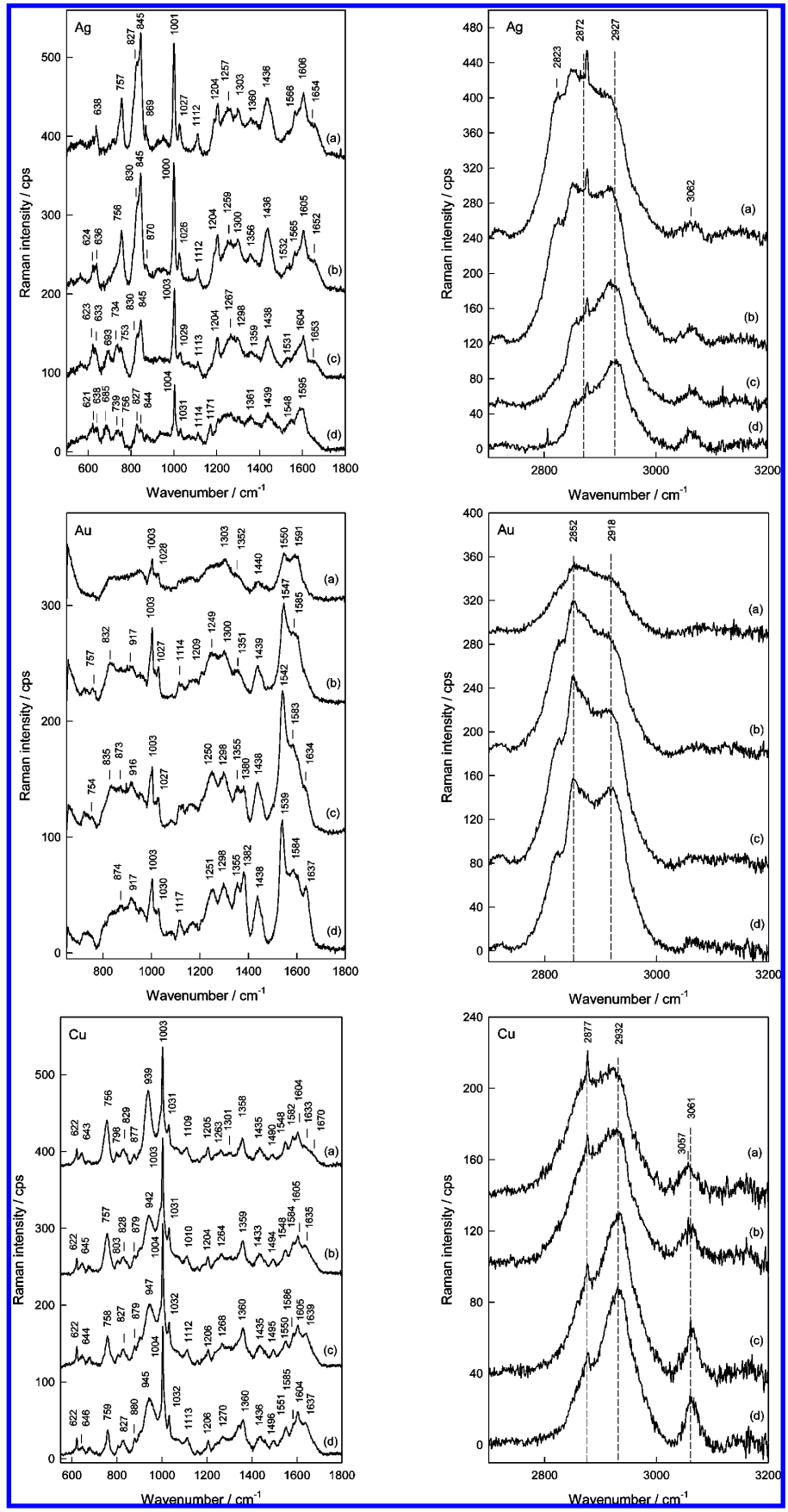

Figure 4. SERS spectra of [D-Phe^6,β-Ala^{11},Phe^{13},Nle^{14}]BN$^{6-14}$ adsorbed on roughened (A) Ag electrode at potentials of −1.200 V (a), −0.800 V (b), −0.400 V (c), and 0.000 V (d); (B) Au electrode at potentials of −1.200 V (a), −0.800 V (b), −0.400 V (c), and 0.000 V (d); and (C) Cu electrode at potentials of −1.200 V (a), −0.800 V (b), −0.600 V (c), and −0.400 V (d). Measurement conditions are as follows: 0.1 M Na_2SO_4 solution containing 0.01 M phosphate buffer (pH 7.0) and 10^{-5} M peptide; excitation wavelength, 785 nm; laser power at the sample, 50 mW; integration time, 1500 s.

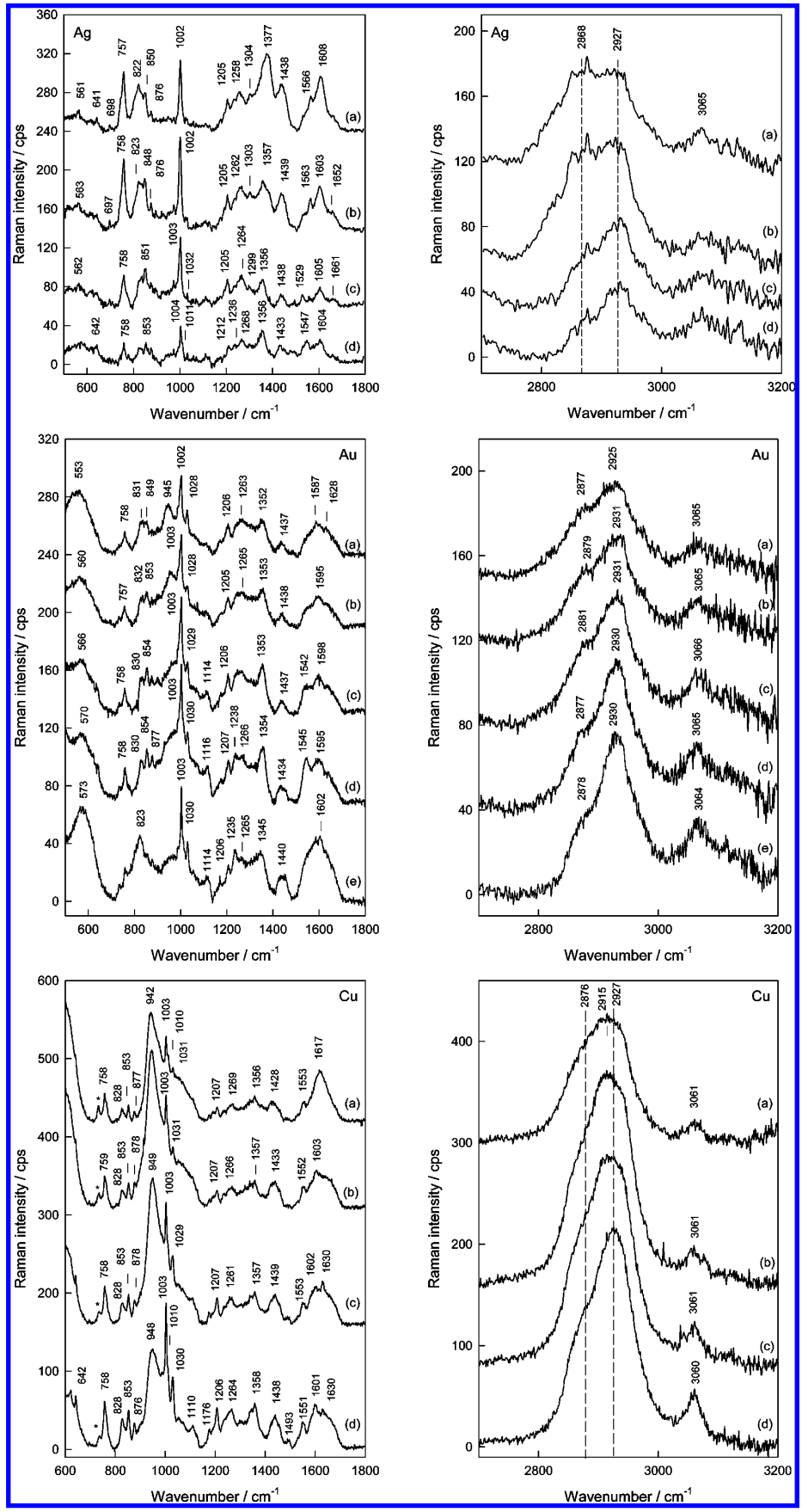

Figure 5. SERS spectra of [D-Tyr^6,β-Ala^{11},Phe^{13},Nle^{14}]BN$^{6-14}$ adsorbed on roughened (A) Ag electrode at potentials of −1.200 V (a), −0.800 V (b), −0.400 V (c), and 0.000 V (d); (B) Au electrode at potentials of −1.200 V (a), −0.800 V (b), −0.400 V (c), 0.000 V (d), and 0.400 V (e); and (C) Cu electrode at potentials of −1.200 V (a), −1.000 V (b), −0.800 V (c), and −0.600 V (d). Measurement conditions are as follows: 0.1 M Na_2SO_4 solution containing 0.01 M phosphate buffer (pH 7.0) and 10^{-5} M peptide; excitation wavelength, 785 nm; laser power at the sample, 50 mW; integration time, 1500 s.

at the same excitation wavelength (785 nm).[34,37] This supports our earlier results demonstrating that (i) the adsorption mechanism of BN on roughened Ag, Au, and Cu electrode surfaces is analogous to that on the surface of silver nanoparticles,[37] (ii) the first five amino acids of the BN N-terminus do not influence the adsorption mechanism on the Ag substrates, and (iii) a preferential interaction between the phenylalanine residue and the Ag sol is observed over that between Trp[8] and this substrate.[37]

The spectra of adsorbed BN[6−14] fragments on the Ag, Au, and Cu electrode surfaces are also similar to one another, both in spectral pattern and in their band positions. However, they differ in relative band intensities. The most distinct differences lie in the spectral features assigned to ν(C−C), ν_s(C−N−C), and AII/W4, at ∼845, 827, and 1539 cm^{-1}, respectively. While strong in the SERS spectra of [D-Phe[6],β-Ala[11],Phe[13],Nle[14]]BN[6−14] immobilized on the Ag electrode surface, they almost disappear in the SERS spectra of this fragment on the Au and Cu electrodes (Figure 4). In addition, a marked decrease in surface enhancement of the W band (∼680 cm^{-1}) is evident for [D-Phe[6],Leu-NHEt[13],des-Met[14]]BN[6−14] on the Ag and Cu electrode surfaces. For some BN[6−14] fragments, another interesting phenomenon involves the positions of the bands due to vibrations in the D-Phe and Trp[8] residues. These bands coincide with the wavenumbers of the corresponding bands in the normal Raman spectra to within 1−2 cm^{-1}. They are also comparatively narrow, suggesting that there is no direct interaction between these residues and the Ag, Au, or Cu substrates. However, downward shift of the Phe ring stretching mode from 1004 to 1001 cm^{-1} was detected for [D-Phe[6],β-Ala[11],Phe[13],Nle[14]]BN[6−14] adsorbed at the Ag electrode at negative potentials (Figure 4A). Usually, the position of this band is very stable; therefore, a small but reliable decrease in frequency may serve as an indication of the specific interaction of Phe with the Ag surface. A similar shift was not observed for Au and Cu electrodes. Variation in the parameters of the W18 band of Trp[8] (near 759 cm^{-1}) was also detected. Broadening of this mode, decrease in frequency, and increase in intensity were the factors indicating specific interaction of the indole ring with the electrode surface.

Some specific differences between the potential-dependent spectra on Ag, Au, and Cu can clearly be observed for the BN[6−14] fragments investigated. For instance, for cyclo[D-Phe[6],His[7],Leu[14]]BN[6−14] deposited onto the roughened Ag electrode (Figure 1A), the bands at 759 and 1003 cm^{-1}, which are characteristic of the in-plane indole ring breathing vibrations (W18) and ν_{12} of D-Phe[6], respectively, increase slightly in relative intensity when the potential of the Ag electrode becomes more negative. On the other hand, the 1270 (AIII) and 1546 cm^{-1} (W3) bands lose enhancement when the Ag electrode potential becomes more negative. These phenomena are probably caused by subtle variations in the orientation of Trp[8], D-Phe[6], and the peptide bond on the Ag electrode surface when the electrode potential becomes more negative. Considering the above spectral alternations and the fact that spectra of cyclo[D-Phe[6],His[7],Leu[14]]BN[6−14] on an Ag electrode are dominated by bands at 1003, 1270, 1304 (W8/$\delta_{i.p.}$(CH)/ρ_t(CH$_2$)), 1350 (W7), 1436 (W6/δ_{as}(CH$_3$)/δ(CH$_2$)), and 1601 cm^{-1} (Phe (ν_{8a})) (see Table 1 for detailed band allocations), a reorientation can be proposed when the electrode potential becomes more negative. Specifically, in close proximity to the Ag electrode surface, (i) the rearrangement of the indole ring simultaneously weakness its pyrrole coring···Ag interaction and strengthens its phenyl coring···Ag interaction; (ii) the nearly flat D-Phe[6] ring on the Ag electrode surface rises slightly; and (iii) the peptide bond accepts a more parallel orientation with respect to the Ag electrode surface and thus more strongly interacts with this surface. These conclusions are further supported by the lack of down-shift in wavenumber, the 5 cm^{-1} band broadening of the ∼1003 cm^{-1} SERS band in the electrode potential range of −1.200 and 0.000 V (in comparison to the positions and width of this band in the normal Raman spectrum of neat solid state cyclo[D-Phe[6],His[7],Leu[14]]BN[6−14], namely, 1004 cm^{-1} and fwhm = 8 cm^{-1} (fwhm = full width at half-maximum), respectively), and the ∼10 cm^{-1} position lowering of the amide III SERS signal.

The differences described above can be detected successfully for isolated bands using simple spectral analysis because the relative intensity variations are sufficiently pronounced. If the relative intensity changes are very small, generalized two-dimensional correlation analysis can be applied. This novel G2D-correlation method is useful for analyzing spectral signals that change as a function of many kinds of reasonable physical variables which affect the spectra, such as time, temperature, concentration, potential, pressure, and even chemical reaction.[40,49−51] Therefore, in order to study subtle differences in the profile of the cyclo[D-Phe[6],His[7],Leu[14]]BN[6−14] SERS spectra (Figure 1), we performed G2DCA using changes of the electrode potential as a variable.

Figure 6 presents synchronous (on left) and asynchronous (on right) G2D-correlation maps in the 1700−600 cm^{-1} wavenumber range, generated from the potential-dependent SERS spectra of cyclo[D-Phe[6],His[7],Leu[14]]BN[6−14] deposited onto the roughened Ag, Au, and Cu electrodes. The synchronous map for this fragment on Ag (Figure 6A, on left) contains two very strong ((1546,1546) and (1270,1270) cm^{-1}) and two low intensity ((1003,1003) and (759,759) cm^{-1}) autopeaks. The strong intensity of the (1546,1546) and (1270,1270) cm^{-1} peaks suggests that the enhancement of these bands changes most significantly with changes in electrode potential. The lack of peaks located at the diagonal positions, which would represent the remaining SERS signals in these spectra on Ag, imply that there is no relative intensity shift of these bands for electrode potentials between −1.200 and 0.000 V.

In addition to the autopeaks, four negative cross-peaks at (759,1546), (759,1270), (1003,1546), and (1003,1270) cm^{-1} are present in the synchronous spectrum. The negative sign of these cross-peaks indicates that all of these SERS signals undergo potential-dependent enhancement changes in the reverse direction. This supports previous observations. The asynchronous map also develops several cross-peaks (Figure 6A, on right). The appearance of these peaks in the asynchronous map suggests that the directions of the transition moments of these modes are different. The positive signs of the most prominent peaks at (824,1546), (1003,1546), and (1546,1590) cm^{-1} indicate that the potential-induced spectral changes at 824 and 1003 cm^{-1} take place earlier than those at 1546 cm^{-1}, and similarly, those at 1546 cm^{-1} take place earlier than those at 1590 cm^{-1}. On the other hand, the negative sign of the (1270,1546) cm^{-1} peak suggests that spectral changes take place earlier at 1546 cm^{-1} than at 1270 cm^{-1}.

Several important differences in the relative intensity of the previously discussed spectral features are observed in going from the SERS spectra (Figure 1A) and G2D-correlation maps (Figure 6A) of cyclo[D-Phe[6],His[7],Leu[14]]BN[6−14] adsorbed on the roughened Ag electrode to the SERS spectra (Figure 1B) and the G2D-correlation maps (Figure 6B) of this fragment immobilized on the Au electrode surface. For example, the most intense autopeaks of the synchronous G2D-correlation map of cyclo[D-

TABLE 1: Wavenumbers and Proposed Band Assignments for the RS and SERS Spectra of Phe-Substituted 6−14 Fragments of Amino Acid Adsorbed on Roughened Ag, Au, and Cu Electrode Surfaces[a]

	wavenumber (cm^{-1})																			
	cyclo[D-Phe^6,His^7,Leu^{14}] BN^{6-14}				[D-Phe^6,Leu-NHEt^{13},des-Met^{14}] BN^{6-14}				[D-Phe^6,Leu^{13}-(Ⓡ)-p-Cl-Phe^{14}] BN^{6-14}				[D-Phe^6,β-Ala^{11},Phe^{13},Nle^{14}] BN^{6-14}				[D-Tyr^6,β-Ala^{11},Phe^{13},Nle^{14}] BN^{6-14}			
assignment	RS	Ag (−1.200 V)	Au (−0.400 V)	Cu (−0.400 V)	RS	Ag (−1.200 V)	Au (−1.000 V)	Cu (−1.200 V)	RS	Ag (−1.200 V)	Au (−1.200 V)	Cu (−1.200 V)	RS	Ag (−1.200 V)	Au (0.000 V)	Cu (−1.200 V)	RS	Ag (−1.200 V)	Au (−1.200 V)	Cu (−1.200 V)
$\nu_{as}(NH)_{bonded\ amines}$ or $\nu(NH)_{amides}$					3280								3282							
$\nu_s(NH)_{bonded\ amides}$					3117															
ν(=C−H) in Phe/Trp	3063	3063	3064	3057	3064				3067	3062	3061	3059	3063	3062		3057	3064	3065	3065	3060
$\nu_{as}(CH_3)$	2965				2969				2967				2970				2971			
$\nu(CH_2/CH_3)_{FR}$	2935	2925	2930	2929	2937	2924	2923	2919	2938	2928	2925	2931	2935		2918	2932	2935	2927	2925	2927
								2906												2915
$\nu_s(CH_2/CH_3)$, $\nu_{as}(CH_2)$	2872	2867	2873	2880	2876	2880	2875	2874	2875	2874	2874	2876	2873	2872	2852	2877	2874	2868	2877	2876
										2825	2827			2823						
AI β-turn/unordered	1674				1671								1670			1670				
AI antiparallel β-sheet/α-helix and/or ν(C=O) in Gln^7 $\delta_{as}(NH_2)$		1657	1651	1642		1669		1663	1669	1652		1655		1654	1637	1633	1669	1660		
W1 [phenyl + pyrrole $\nu(N_1-C_8)$]	**1621**				1620	**1614**	**1625**	**1619**	**1617**		**1629[s]**		**1620[s]**				**1617**		**1628**	**1630**
Phe (ν_{8a})/Tyr	*1605*	*1605*	*1596*		*1607*				*1602*	*1606*		*1600*	*1605*	*1606*		*1604*	*1605*	*1608*		*1601*
W2 [phenyl] and/or *Phe (ν_{8b})*	**1580**			**1581**	**1579**		**1586**	**1582**	**1585**	**1566**	**1585**	**1583**	**1585**		**1584**	**1582**	**1583**		**1587**	
									1578											
W3 [pyrrole $\nu(C_2=C_3)$]	**1555**	**1564**	**1549**		**1553**	**1566**		**1551**	**1555**		**1548**	**1550**	**1555**	**1566**	**1539**	**1548**	**1553**	**1566**		**1551**
AII and/or **W4 [phenyl ν(C=C)]**						**1531**														
disubstituted aromatic ring	1493	1486		1491	1493	1492			1493	1490	1486	1489				1490	1494			1493
W5 [phenyl] and $\rho_s(CH_2)$	**1459**				**1458**				**1459**	**1438**	**1434**	**1439**	**1457**							
W6 [pyrrole ($\nu_s(N_1C_2C_3)$ + $\delta(N_1-H)$) + phenyl δ(CH)], $\delta_{as}(CH_3)$, and/or $\delta(CH_2)$	**1448**	**1441**	**1442**		**1435**	**1436**	**1445**	**1439**	**1429**				**1436**	**1436**	**1438**	**1435**	**1458**	**1438**	**1437**	**1438**
	1432																**1436**			
ν(C=O) in Gln^7				1391											1382					
W7 [pyrrole ring $\nu(N_1-C_8)$; Fermi resonance] and/or $\rho_w(CH_2)$	**1359**	**1365**	**1355**	**1345**	**1361**	**1356**	**1341**	**1359**	**1361**	**1358**	**1358**	**1359**	**1362**	**1360**	**1355**	**1358**	**1361**	**1377**	**1352**	**1358**
	1342				**1337**			**1340**	**1340**				**1337**				**1340**			**1344**
$\delta_{i.p.}(CH)$, $\rho_t(CH_2)$, and/or **W8 [$\nu(C_3-C_9)$ + $\delta(N_1-H)$]**		1303	1307	1289	1298	1308				1299	1302	1314	1281	1303	1298	1301	1302	1304		
																	1281			
AIII, *Phe (ν_3)*, and/or $\delta(CC_\alpha H)$	1262	1260	1265	1252	1255	1258	1268	1266	1262	1253	1250	1262	1251	1257	1251	1263	1251	1258	1263	1264
W10 [$\nu(C_3-C_\beta H_2)$ + ν(C−H)] and/or $\rho_t(CH_2)_{Trp}$					**1237**		**1238**	**1237**	**1238**				**1235**				**1234**			
Phe (ν_{7a})	*1204*				*1205*				*1207*	*1205*	*1205*	*1206*	*1206*	*1204*	*1206*	*1205*	*1207*	*1205*	*1206*	*1206*
$\delta(N_1H)$, $\rho_t(NH_2)$ in Asn/Gln, and/or *Phe (ν_{9a})*			**1171**		**1187**		**1174**		**1183**	**1186**	**1182**	**1183**	**1187**		**1171**					**1176**
									1159			**1157**	**1158**							
$\rho_t(NH_2)$ in Asn and/or phosphate anions	1127	1125	1116	1114	1127		1126		1129	1112	1111	1109	1127	1112	1117	1109	1126			1110
$\nu(C-C)_T$ alkyl chain and/or **W13 [phenyl]**, ν(C−N), and/or $\rho_t(CH_2)$		1108							1094		1090		1081							
													1064							

TABLE 1 Continued

	wavenumber (cm^{-1})																			
	cyclo[D-Phe^6,His^7,Leu^{14}] BN$^{6-14}$				[D-Phe^6,Leu-NHEt^{13},des-Met^{14}] BN$^{6-14}$				[D-Phe^6,Leu^{13}-(Ⓡ)-p-Cl-Phe^{14}] BN$^{6-14}$				[D-Phe^6,β-Ala^{11},Phe^{13},Nle^{14}] BN$^{6-14}$				[D-Tyr^6,β-Ala^{11},Phe^{13},Nle^{14}] BN$^{6-14}$			
assignment	RS	Ag (−1.200 V)	Au (−0.400 V)	Cu (−0.400 V)	RS	Ag (−1.200 V)	Au (−1.000 V)	Cu (−1.200 V)	RS	Ag (−1.200 V)	Au (−1.200 V)	Cu (−1.200 V)	RS	Ag (−1.200 V)	Au (0.000 V)	Cu (−1.200 V)	RS	Ag (−1.200 V)	Au (−1.200 V)	Cu (−1.200 V)
ν(C−C)$_T$ alkyl chain, guanido group of Arg, and/or ρ_t(CH_2)																	1083			
																	1063			
Phe (ν_{18a})	*1032*	*1030*	*1032*	*1031*	*1033*		*1028*		*1032*	*1028*	*1028*	*1030*	*1032*	*1027*	*1030*	*1031*	*1031*	*1032*	*1028*	*1030*
W16 [phenyl and pyrrole ring out-of-phase breathing]	**1011**	**1011^S**	**1010^S**		**1011**			**1011**	**1012**				**1011**				**1012**	**1011^S**		**1010**
Phe (ν_{12})	*1004*	*1003*	*1003*	*1003*	*1004*	*1003*	*1002*		*1004*	*1002*	*1003*	*1003*	*1004*	*1001*	*1003*	*1003*	*1003*	*1002*	*1002*	*1003*
ν(C−N), ρ_b(NH_2), and/or phenyl ρ_b(CH)							988													
phosphate anions	961	940	956	942		947	946	947	962		956	937	893		917	939			945	948
									907											
W17 [indole + ρ_b(N_1−H) and Fermi resonance between phenyl ring breathing and oop ring bend overtone]	**879**	**878**	**877^S**	**877**	**876**	**877**	**881**	**878**	**879**	**874**	**876**	**877**	**879**	**869**	**874**	**877**	**892**	**876**		**876**
																	878			
Tyr doublet																	853	850	849	853
																	833	822	831	828
ν(C−C) and/or ν_s(CNC) secondary amide	831	824	838		830		832	831	832	826	828		832	845		829				
														827						
ν(C−C)									810			795				798				
W18 [sym phenyl/pyrrole ring breathing]	**759**	**758**	**758**	**758**	**758**	**758**	**757**	**758**	**759**	**757**	**759**	**757**	**760**	**757**	**757**	**756**	**759**	**757**	**758**	**758**
W19	721				723	746	729		722	745			724		734		723			
W, δ(NCO), and/or δ(COO)		**697**					**680**											**698**		
δ(NCO) and/or δ(COO)									634	637		647		638		643	643	641		642
Phe (ν_{6b})	*622*				*622*				*622*	*622*		*622*	*622*			*622*	622			

[a] Abbreviations: ν, stretching; δ, deformation; ρ_w, wagging; ρ_b, bending; ρ_t, twisting; subscript "s", symmetric; subscript "as", asymmetric; subscript "oop", out of plane; subscript "ip", in-plane vibrations; superscript "s", shoulder; FR, Fermi resonance.

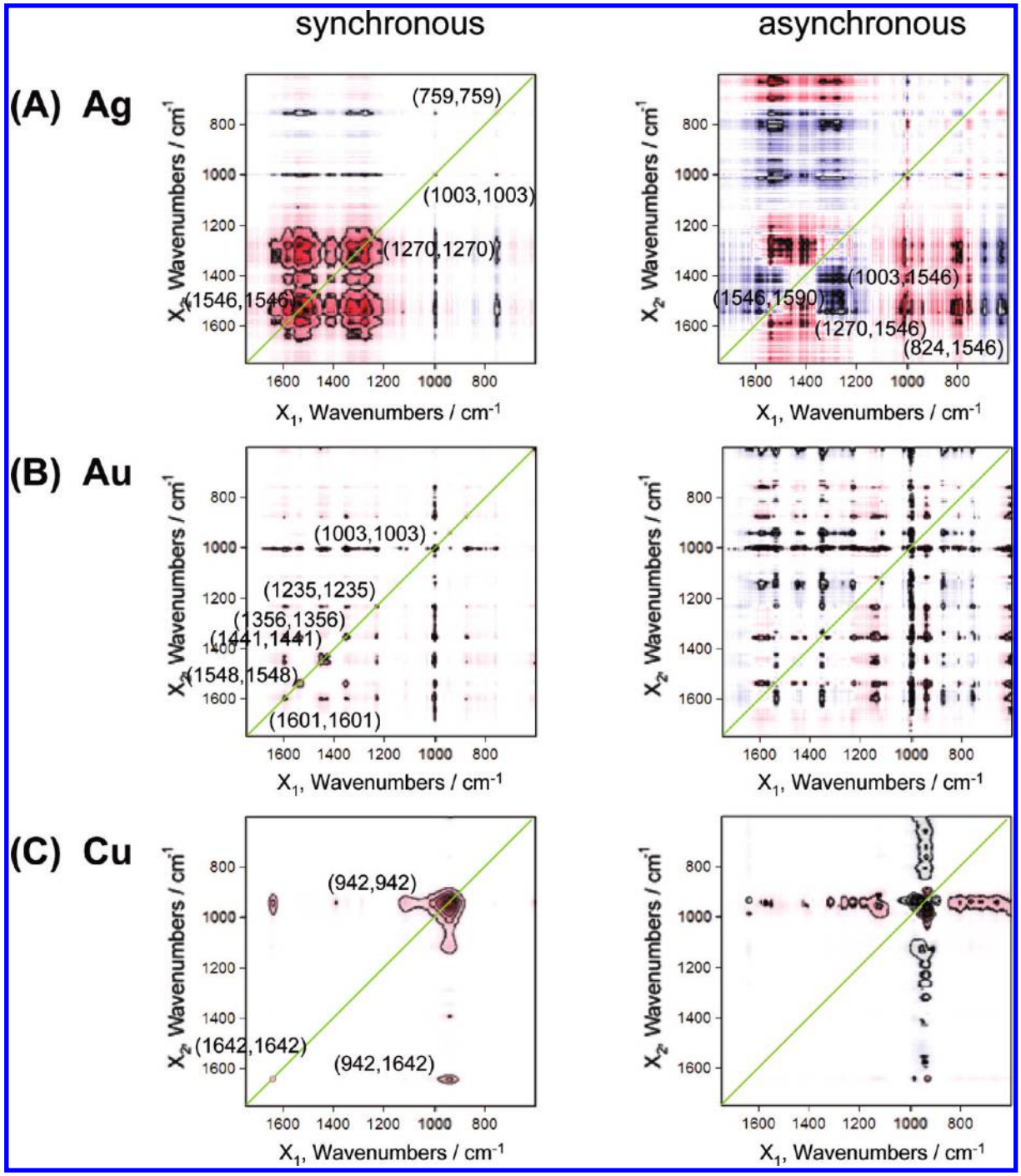

Figure 6. Generalized synchronous (left) and asynchronous (right) 2D-correlation maps of the SERS spectra of cyclo[D-Phe^6,His^7,Leu^{14}]BN$^{6-14}$ adsorbed on roughened Ag, Au, and Cu electrodes as a function of electrode potential, within the spectral range 1700−600 cm^{-1}.

Phe^6,His^7,Leu^{14}]BN$^{6-14}$ on Au (Figure 6B, on left) are (1003,1003) and (1441,1441) cm^{-1}. This means that instead of the 1546 and 1270 cm^{-1} bands, the enhancement of the 1003 and 1441 cm^{-1} SERS signals is most prominently reduced when the roughened Au electrode potential becomes less positive. Note also that the autopeaks at (1270,1270) and (759,759) cm^{-1} of the synchronous G2D-correlation map on Ag (Figure 6A, on left) disappear and nearly disappear, respectively. Instead, the (1601,16001), (1441,1441), (1356,1356), and (1235,1235) cm^{-1} autopeaks emerge (see Table 1 for band allocations). These data indicate that cyclo[D-Phe^6,His^7,Leu^{14}]BN$^{6-14}$ assumes a slightly different structure on the Au electrode, compared with the Ag electrode, when the electrode potential becomes more negative. Several positive cross-peaks are also observed, i.e., (1003,1235), (1003,1356), (1003,1441), (1003,1548), (1003,1601), (1441,1601), (1356,1548), (1235,1601), and (1235,1441) cm^{-1} (Figure 6B, left), suggesting that the relative intensities of these spectral features change in the same manner. On the other hand, the asynchronous G2D-correlation map of cyclo[D-Phe^6,His^7,Leu^{14}]BN$^{6-14}$ on Au (Figure 6B, on right) clearly shows that the change at 1003 cm^{-1} takes place after those at 1235, 1356, 1441, and 1601 cm^{-1}. Furthermore, the relative intensity changes at 1601 and 1235 cm^{-1} similarly take place before those at 1356 and 1548 cm^{-1}, and finally, enhancement of the 1441 cm^{-1} band is modified before that of the 1548 cm^{-1} band.

These results highlight several possible changes in the adsorption mechanism of cyclo[D-Phe^6,His^7,Leu^{14}]BN$^{6-14}$ on the Au electrode. In particular, the D-Phe^6 ring is tilted with respect

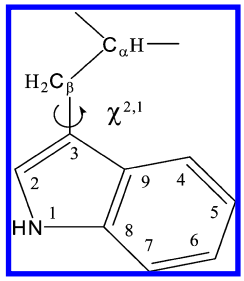

Figure 7. Structure and atom numbering scheme for tryptophan residue.

to the Au surface at 0.400 V. In addition, the indole ring of Trp[8], tilted in close proximity to Au, interacts with this surface mainly through the pyrrole coring. When the Au electrode potential becomes more negative, the tilt angle formed between the phenyl ring and the substrate decreases, so at −1.200 V, it adopts a flat orientation. This is observed as both a marked decrease in relative intensity and breadth (by 4 cm^{-1}) of the 1003 cm^{-1} (I_{1003} ↓) SERS signal, and as a loss of enhancement and down-shift in wavenumber (by 9 cm^{-1}) of the 1601 cm^{-1} spectral feature. At the same time, the interaction strength between the $N_1-C_2=C_3-C_\beta(H_2)$ fragment (see Figure 7 for the structure and atom numbering scheme for the tryptophan residue) and the Au electrode slightly weakens (I_{1235} ↓, I_{1441} ↓, I_{1356} ↓, and I_{1548} ↓) (Figures 1B and 6B). Since the enhancement of the 759 cm^{-1} band is almost insensitive to changes in applied electrode potential, it seems that the reduced strength of the $N_1-C_2=C_3-C_\beta(H_2)\cdots$Au interaction is a consequence of a reorientation of D-Phe[6], which pushes Trp[8] away from the Au surface slightly. Finally, the peak associated with the phenyl-ring C−H stretching vibration near 3064 cm^{-1} decreases in intensity for less negative electrode potentials (Figure 1, on right), supporting the suggestion that the phenyl ring moves from a tilted orientation with respect to the Au surface at −1.200 mV to a flat geometry at 0.400 V.[52]

The behavior of the amide signals in the SERS spectra of cyclo[D-Phe[6],His[7],Leu[14]]BN^{6-14} on the Au electrode (Figures 1B and 6B) is quite different from that observed on the Ag substrate. First, the relative intensity of the amide I and III bands (see Table 1 for positions) does not change when the electrode potential becomes more negative, indicating that the −CONH− bond orientation with respect to the Au surface also does not change. Second, these SERS signals do not shift in wavenumber compared with those signals observed in the normal cyclo[D-Phe[6],His[7],Leu[14]]BN^{6-14} Raman spectrum (Table 1). By comparison, the 7−10 cm^{-1} movement to lower wavenumber of the amide I and III bands in the SERS spectra on Ag are indicative of conformational heterogeneity of −CONH− on Ag and homogeneity on Au.

The positions and relative intensities of the SERS signals of cyclo[D-Phe[6],His[7],Leu[14]]BN^{6-14} on the Cu electrode (Figure 1C) at different electrode potentials also seem to be potential-dependent. Similar conclusions can be drawn when analyzing the G2D-correlation maps (Figure 6C) generated from these spectra, which show one very strong (at (942,942) cm^{-1}) autopeak belonging to the SERS signal of adsorbed phosphate anions and one very weak autopeak (at (1642,1642) cm^{-1}), probably due to the ν(C=O) mode.[48] Additionally, a few weak positive cross peaks at (942,1642), (942,1390), and (942,1345) cm^{-1} are nevertheless traceable. Thus, the most notable differences in these spectra are related to the amide I (1642 cm^{-1}) and ν(C=O) (1391 cm^{-1}) vibrations, as well as those of amide III (1252 cm^{-1}) and W18 (758 cm^{-1}) (see Table 1 for detailed band positions). At −0.400 V, the first above-mentioned SERS signal is strongly enhanced and reduced in wavenumber by 32 cm^{-1}, compared with the neat Raman spectrum of this fragment, indicating direct interaction of the C=O fragment of −CONH− with the Cu electrode surface. This can be supported by the moderate enhancement of the ν(C=O) mode and weak relative intensity of the amide III band. When the electrode potential becomes more negative, the 1642 and 1391 cm^{-1} spectral features markedly lose their enhancement, whereas the 1252 cm^{-1} feature shifts up in wavenumber (by 14 cm^{-1}) without any relative intensity change. This may imply that, at more negative electrode potentials, the amide bond$\cdots$Cu interaction is no longer direct.

Furthermore, the orientation of Trp[8] on Cu is sensitive to the applied electrode potential. At more positive Cu electrode potentials, the lone pair of electrons in the N_1-C_8 unit interacts with the Cu surface, while at less positive potentials the indole ring (758, 1345, and 1437 cm^{-1}) interacts with this surface.

The contribution of the $-CH_2-/-CH_3$ units to the SERS spectra of cyclo[D-Phe[6],His[7],Leu[14]]BN^{6-14} deposited onto roughened Ag, Au, and Cu electrodes (Figure 1) is composed of strong intensity bands at around 2925−2930 and 2867−2880 cm^{-1}. These are due to the asymmetric and symmetric stretching vibrations of the C−H bond, respectively. The relative intensity of the latter feature increases for cyclo[D-Phe[6],His[7],Leu[14]]BN^{6-14} on all electrode surfaces when the electrode potential becomes more negative.

For the other four BN^{6-14} fragments investigated, slight substrate-dependent and potential-dependent spectral variations are observed (Figure 2−4), and these are highlighted in the G2D-correlation maps (Figure 8−11). In the SERS spectra of [D-Phe[6],Leu-NHEt[13],des-Met[14]]BN^{6-14} (Figure 2A) and [D-Phe[6],Leu[13]-(Ⓡ)-p-Cl-Phe[14]]BN^{6-14} (Figure 3A) on the Ag electrode, the ∼1003 and 757 cm^{-1} bands visibly decrease in their relative intensities when the electrode potential becomes more positive. The synchronous G2D-correlation maps of these fragments (Figures 8A and 9A, respectively) contain only two autopeaks, of pronounced relative intensity, and one strong positive cross-peak (at (757,1003) cm^{-1}) that corresponds to the above two SERS signals. However, the synchronous G2D-correlation map of [D-Phe[6],Leu[13]-(Ⓡ)-p-Cl-Phe[14]]BN^{6-14} (Figure 9A, on left) shows one barely visible autopeak (at (1566,1566) cm^{-1}) and one low intensity positive cross-peak (at (1002,1566) cm^{-1}). These peaks highlight the changes observed in the SERS spectra and emphasize that the direction of intensity shift is the same (a decrease). These facts also imply that the rest of the enhanced SERS bands in these SERS spectra are independent of the applied electrode potential.

The asynchronous G2D-correlation map of [D-Phe[6],Leu-NHEt[13],des-Met[14]]BN^{6-14} (Figure 8A, on right) shows five distinct positive and two negative peaks. This reveals that the changes at 1003 and 757 cm^{-1} take place earlier than those at 877, 1356, and 1492 cm^{-1}, while the transition at 1003 cm^{-1} takes place after that at 1566 cm^{-1}. These observations agree with results obtained from the asynchronous G2D-correlation map of [D-Phe[6],Leu[13]-(Ⓡ)-p-Cl-Phe[14]]BN^{6-14} (Figure 9A, on right). The latter suggests that the change at 1566 cm^{-1} happens before those at 1002 and 757 cm^{-1}, whereas the change at 1002 cm^{-1} follows that at 757 cm^{-1}.

The above data suggest analogous behavior between [D-Phe[6],Leu-NHEt[13],des-Met[14]]BN^{6-14} and [D-Phe[6],Leu[13]-(Ⓡ)-p-Cl-Phe[14]]BN^{6-14} on Ag. It may be proposed that, at an Ag electrode potential of −1.200 V, both of these BN^{6-14} fragments adsorb mainly via the nearly vertical pyrrole coring of Trp[8],

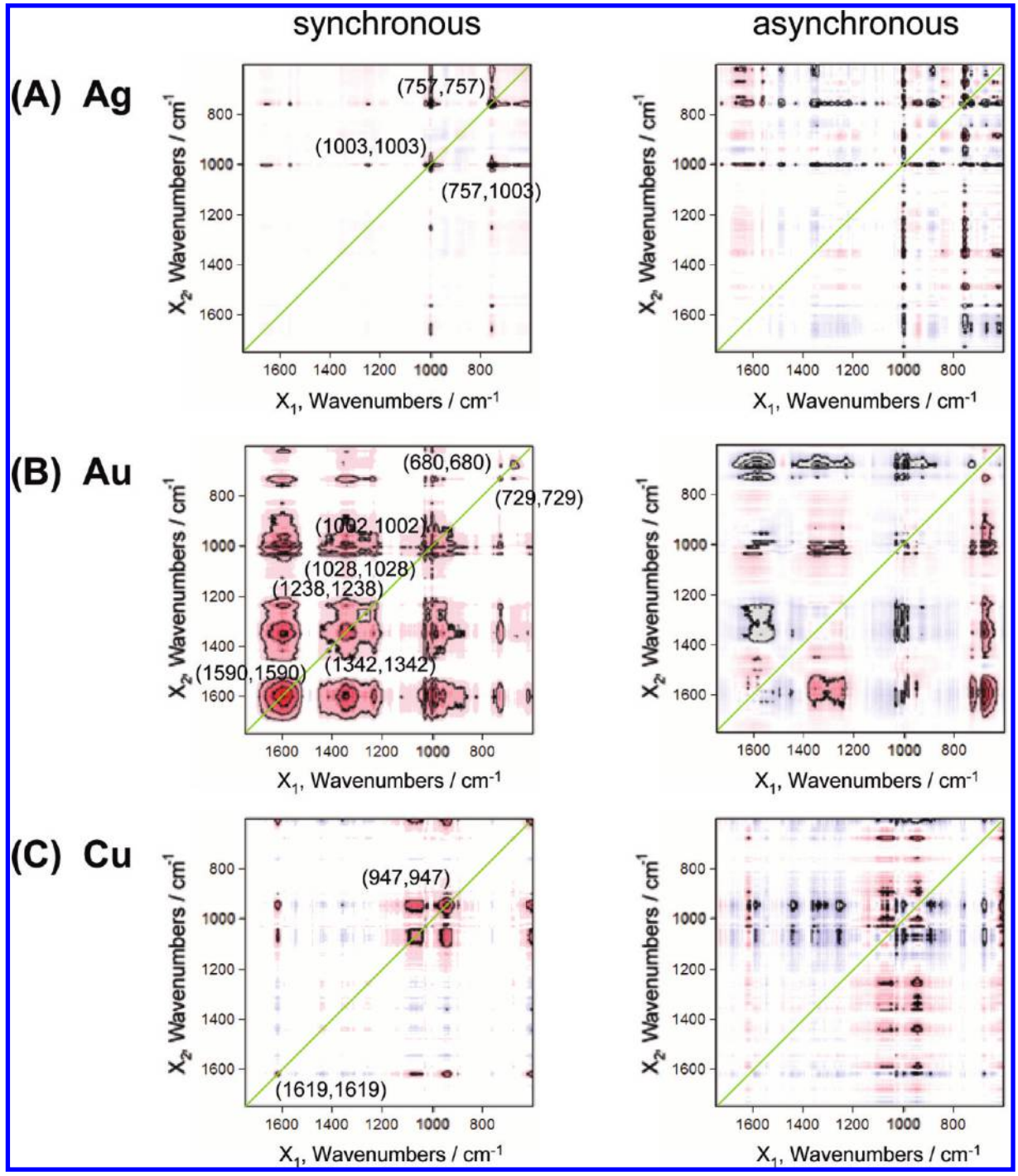

Figure 8. Generalized synchronous (left) and asynchronous (right) 2D-correlation maps of the SERS spectra of [D-Phe^6,Leu-NHEt^{13},des-Met^{14}]BN$^{6-14}$ adsorbed on roughened Ag, Au, and Cu electrodes as a function of electrode potential, within the spectral range 1700−600 cm^{-1}.

the tilted D-Phe^6 ring, and the amide bond. However, the movement of the indole ring with respect to the surface normal is somewhat higher for [D-Phe^6,Leu-NHEt^{13},des-Met^{14}]BN$^{6-14}$ than for [D-Phe^6,Leu^{13}-(Ⓡ)-p-Cl-Phe^{14}]BN$^{6-14}$, and the relative SERS intensity of the 1003 cm^{-1} band for [D-Phe^6,Leu-NHEt^{13},des-Met^{14}]BN$^{6-14}$ is one-fourth higher than that of [D-Phe^6,Leu^{13}-(Ⓡ)-p-Cl-Phe^{14}]BN$^{6-14}$ at −1.200 V. When the electrode potential is decreased to 0.000 V, the D-Phe^6 ring adopts a flat orientation on the Ag surface, and the indole ring tilts toward this surface. The strength of the pyrrole coring···Ag interaction is constant for [D-Phe^6,Leu-NHEt^{13},des-Met^{14}]BN$^{6-14}$, while it diminishes a little for [D-Phe^6,Leu^{13}-(Ⓡ)-p-Cl-Phe^{14}]BN$^{6-14}$.

In the SERS spectra of [D-Phe^6,Leu-NHEt^{13},des-Met^{14}]BN$^{6-14}$ on Au (Figure 2B), many more changes in the relative band intensities can be observed when the electrode potential is changed, in comparison to the number of changes seen for this fragment adsorbed on Ag (Figure 2A) and for [D-Phe^6,Leu^{13}-(Ⓡ)-p-Cl-Phe^{14}]BN$^{6-14}$ immobilized on Au (Figure 3B). These spectral alterations are observed in the 680, 1002, 1028, 1238, 1342, and 1590 cm^{-1} bands (see Table 1 for band allocation). The proper corresponding auto- and cross-peaks in the G2D-correlation maps of [D-Phe^6,Leu-NHEt^{13},des-Met^{14}]BN$^{6-14}$ on Au are shown in Figure 8B. Both from the relative intensity analysis of the SERS spectra and from the positive sign of all of the cross-peaks in the synchronous G2D-correlation map, it may be deduced that all of these bands lose surface enhancement when the electrode potential becomes more positive. Moreover, analyzing the asynchronous G2D-correlation map of this frag-

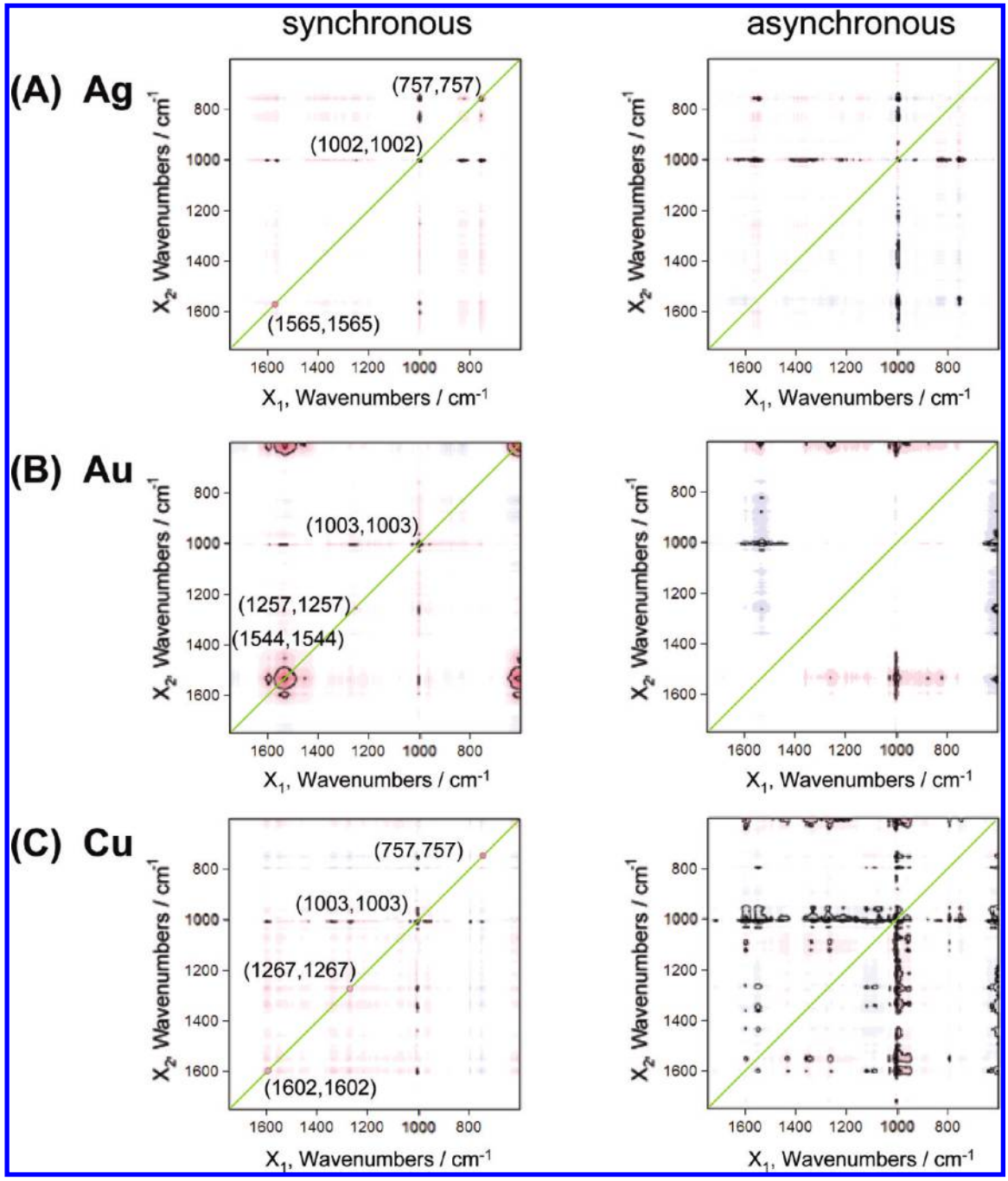

Figure 9. Generalized synchronous (left) and asynchronous (right) 2D-correlation maps of the SERS spectra of [D-Phe^{6},Leu^{13}-(Ⓡ)-p-Cl-Phe^{14}]BN$^{6-14}$ adsorbed on roughened Ag, Au, and Cu electrodes as a function of electrode potential, within the spectral range 1700−600 cm^{-1}.

ment (Figure 8B, on right) shows that the first transition takes place at 680 cm^{-1}, followed by those at 1590, 1342, 1238, 1028, 1002, and 729 cm^{-1}. However, the changes at 1342 and 1238 cm^{-1} take place before those at 1590 cm^{-1}, and the change at 1028 cm^{-1} follows those at 1342 and 1238 cm^{-1}. The following possible picture of SERS profile alternation for [D-Phe^{6},Leu-NHEt^{13},des-Met^{14}]BN$^{6-14}$ on the Au electrode surface may be used to explain the data. When the Au electrode potential become more positive (−1.200 V → 0.400 V), the more or less flat indole ring sitting in close proximity to the surface stands up in a manner whereby the phenyl and pyrrole corings remain in unchanged contact with the Au electrode surface. At the same time, the D-Phe^{6} ring, originally almost flat on the Au, lifts slightly. During these rearrangements, the amide bond does not change its orientation on this surface.

The SERS spectra of [D-Phe^{6},Leu-NHEt^{13},des-Met^{14}]BN$^{6-14}$ on the Cu electrode (Figure 2C), in comparison to spectra on Ag (Figure 2A) and Au (Figure 2B), clearly show one additional SERS band at 1011 cm^{-1} (W16) of relative intensity comparable to the Raman intensity, which overlaps the Phe (ν_{12}) mode (shoulder at 1003 cm^{-1}). Like other bands observed on this fragment, these two bands do not change their wavenumbers or relative intensities when the electrode potential is changed (see Figure 8C). Therefore, we suggest that [D-Phe^{6},Leu-NHEt^{13},des-Met^{14}]BN$^{6-14}$ does not change its structure as a function of electrode potential. In this structure, the D-Phe^{6} ring is flat, whereas the indole ring, tilted close to flat, lies closer to the Cu surface than to the Ag or Au surfaces.

In the potential-dependent SERS spectra of [D-Phe^{6},Leu^{13}-(Ⓡ)-p-Cl-Phe^{14}]BN$^{6-14}$ on Au (Figure 3B) and Cu (Figure 3C)

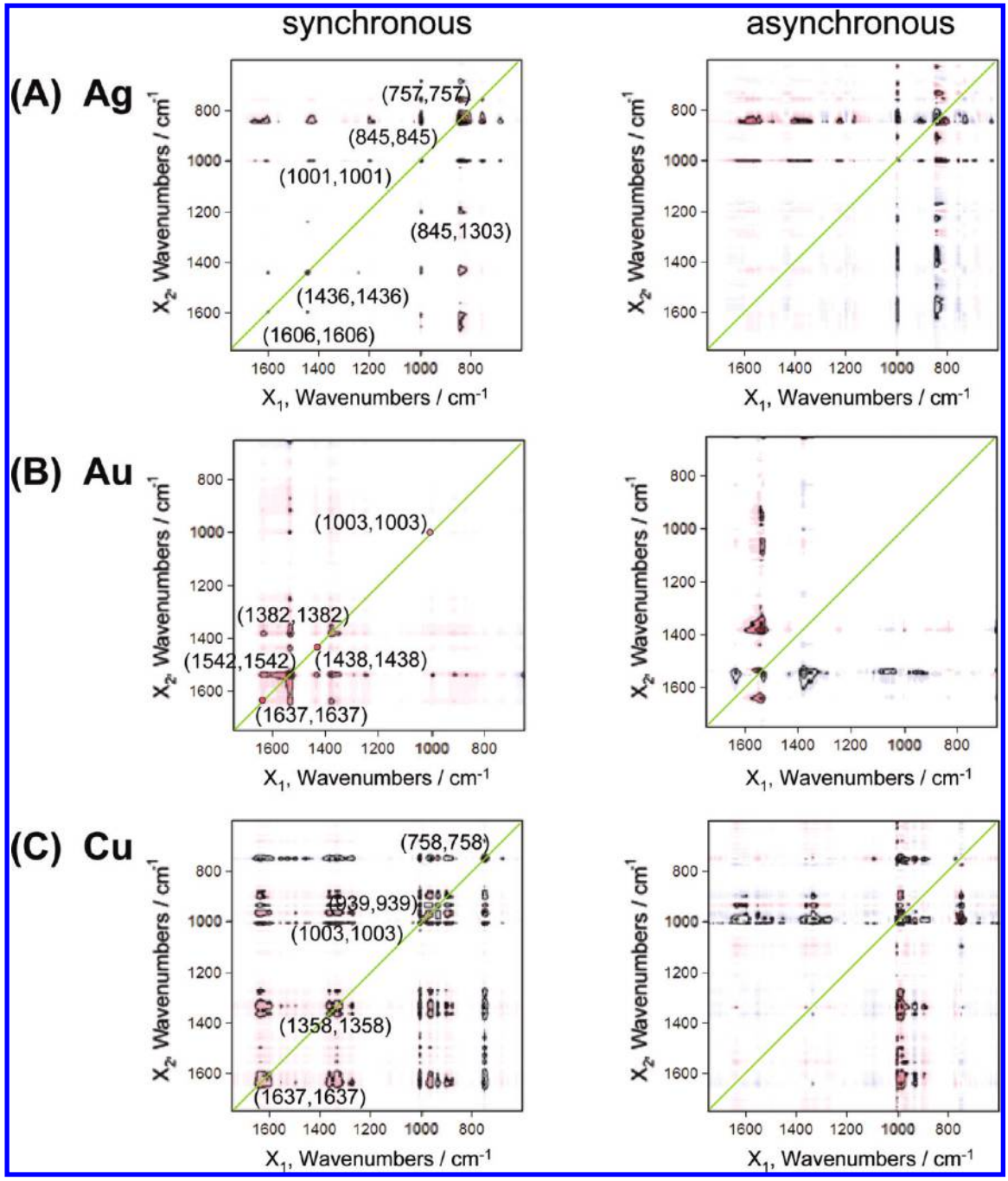

Figure 10. Generalized synchronous (left) and asynchronous (right) 2D-correlation maps of the SERS spectra of [D-Phe^6,β-Ala^{11},Phe^{13},Nle^{14}]BN$^{6-14}$ adsorbed on roughened Ag, Au, and Cu electrodes as a function of electrode potential, within the spectral range 1700−600 cm^{-1}.

electrodes, only three subtle variations in surface enhancement are observed with potential change. These features are observed at 1544, 1257, and 1003 cm^{-1} in the case of Au and at 1602, 1267, and 1003 cm^{-1} in the case of Cu. These changes are clearly visible as auto- and positive cross-peaks in the G2D-correlation maps on both Au (Figure 9B) and Cu (Figure 9C). The positive cross-peaks in the synchronous maps suggest that all intensities shift in the same direction. Nevertheless, the positive cross-peaks in the asynchronous maps imply that, on the Au electrode, the change at 1544 cm^{-1} follows those at 1257 and 1003 cm^{-1}, but on Cu, an enhancement change at 1003 cm^{-1} takes place before those at 1602 and 1267 cm^{-1}. Therefore, we conclude that, with an increase of positive charge on the Au electrode, the Trp^8···Au interaction, via the C_2═C_3 fragment, strengthens, reduces the tilt in the orientation of the D-Phe^6 ring with respect to the Au surface, and reorients the amide bond. On the other hand, when the Cu electrode potential becomes more positive, the D-Phe^6 ring rises slightly up toward the surface normal, negligibly altering the orientation of the amide bond on this surface. It should be noted that the W18 band of Trp^8 (near 759 cm^{-1}) broadens and shifts to lower wavenumbers in the case of Cu substrate at more negative electrode potentials (Figure 3A).

The SERS spectra of [D-Phe^6,β-Ala^{11},Phe^{13},Nle^{14}]BN$^{6-14}$ on Ag, Au, and Cu (Figure 4) also show selective band enhancement due to D-Phe^6, Trp^8, and amide bond vibrations, with some relative intensities sensibly different among the spectra on different metal surfaces and at different applied potentials. For example, the rather strong SERS signals observed at 757, 827, 845, 1001, and 1436 cm^{-1} (see Table 1 for band assignment)

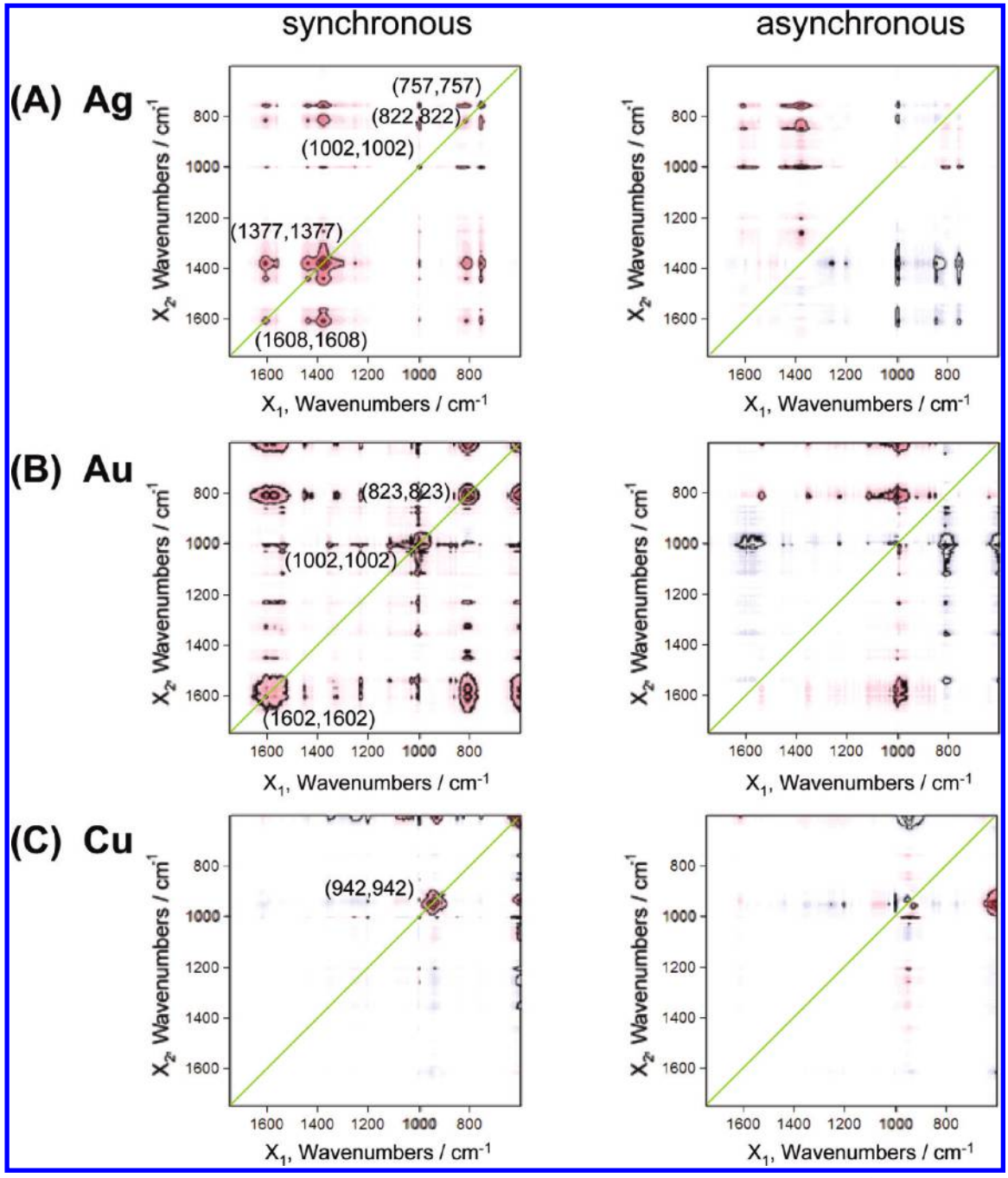

Figure 11. Generalized synchronous (left) and asynchronous (right) 2D-correlation maps of the SERS spectra of [D-Tyr^{6},β-Ala^{11},Phe^{13},Nle^{14}]BN$^{6-14}$ adsorbed on roughened Ag, Au, and Cu electrodes as a function of electrode potential, within the spectral range 1700−600 cm^{-1}.

on the Ag electrode at −1.200 V (Figure 4A) are hardly detectable on the Au electrode (Figure 4B) at the same electrode potential. As the electrode potential increases from −1.200 to 0.000 V, these bands decrease in intensity on Ag, while they increase marginally on Au. Clearly, the Phe ring downshift in wavenumber for the Ag electrode to an unusually low value (1001 cm^{-1}) at −1.200 V points to the specific interaction of the Phe ring with the Ag surface. No such interaction was detected for Au and Cu electrodes. In addition, the bands at 1566−1539 cm^{-1} in the SERS spectra on Ag and Au decrease and increase, respectively, when the electrode potential becomes more positive. The same conclusions can be drawn based on the G2D-correlation maps of this fragment adsorbed on the Ag (Figure 10A) and Au (Figure 10B) electrode surfaces. Further information can be obtained from these maps. From the positive sign of the cross-peaks in the synchronous maps (Figures 10A (on left) and B (on left)), it is clear that the intensities of all of the aforementioned bands shift in the same direction. The relative intensity on Ag at −1.2000 V is comparable to that in the Raman spectrum for this fragment, and since the relative intensities of the 1001 cm^{-1} SERS signal on Ag visibly weaken when the electrode potential becomes more positive, other bands also weaken. The strong relative intensities of the autopeaks in the synchronous maps at 757 cm^{-1} on Ag (Figure 10A (on left)) and at 1542 cm^{-1} on Au (Figure 10B (on left)) indicate the most prominent enhancement changes of these two bands. The negative signs of the (845,1436), (845,1606), (1001,1436), and (1001,1606) cm^{-1} cross-peaks (Figure 10A, on right), as well as the positive sign of the (845,1001) cm^{-1} cross-peak on Ag, suggest that, on the Ag electrode surface, the predominant transition at 1001 cm^{-1} is the last. The transition at 845 cm^{-1} follows slight transitions at 1436 and 1606 cm^{-1}. The negative

sign of the (1382,1542) cm^{-1} cross-peak on Au (Figure 10B, on right) and the positive sign of the (1542,1637) cm^{-1} cross-peak on the Au electrodes suggest that the most pronounced decrease in relative intensity takes place at 1542 cm^{-1}, before two smaller events at 1382 and 1637 cm^{-1}.

All of these observations point to the following scheme of [D-Phe^6,β-Ala^{11},Phe^{13},Nle^{14}]BN$^{6-14}$ reorientation on the Ag and Au electrode surfaces. On the Ag surface at −1.200 V, the D-Phe^6 and Trp^8 (with the N_1—C_2═C_3 fragment oriented toward this surface) rings are normal to the surface. When the electrode potential becomes less negative, both rings fall away from the surface normal. During the rearrangement of these rings, the C—N—C unit shifts its position slightly. On the other hand, on the Au electrode surface at −1.200 V, both the previously discussed aromatic rings and also the peptide bond are almost flat. With an increase in electrode potential up to 0.000 V, reorientation of the amide bond takes place so that it is no longer horizontal to the Au surface. Therefore, it can interact with the surface mainly via the C═O unit of the —CONH— bond (I_{1382} ↑), and thus the amide II band (1542 cm^{-1}) is strongly enhanced. This change forces the D-Phe^6 and Trp^8 rings to rise up a little bit. However, when the indole ring of Trp^8 rises, its N_1—C_2═C_3 fragment is in closer contact with Au than is its phenyl ring.

In the SERS spectra (Figure 4C) and G2D-correlation maps (Figure 10C) of [D-Phe^6,β-Ala^{11},Phe^{13},Nle^{14}]BN$^{6-14}$ adsorbed on the Cu electrode surface, one big (at 757 cm^{-1}, W18) and three small (at 1637, 1358, and 1003 cm^{-1}) changes in signal enhancement due to [D-Phe^6,β-Ala^{11},Phe^{13},Nle^{14}]BN$^{6-14}$ vibrations are observed. On the basis of broadening, peak position shift, and increase in relative intensity of the W18 mode of Trp^8 (Figure 12), we conclude that interaction of the indole ring with the Cu surface takes place at negative electrode potentials. From the positive sign of the cross-peaks in these G2D-correlation maps (Figure 10C), one may see that the 1637, 1358, and 1003 cm^{-1} bands decrease in relative intensity similarly to the peak at 758 cm^{-1}. A distinct change at this wavenumber occurs before a feeble one at 1003 cm^{-1}, which takes place before further changes at 1358 and 1637 cm^{-1}. This mainly supports a reorientation of the Trp^8 ring (evidently, the Trp^8 ring via N_1—C_8 moiety is directed toward the Cu surface) from normal to slightly tilted, when the electrode potential becomes more positive on Cu. Here, the D-Phe^6 ring and amide bond change their orientation only slightly. Evidently, the Trp^8 ring is directed toward the Cu surface via the N_1—C_8 moiety.

Replacement of D-Phe^6 in [D-Phe^6,β-Ala^{11},Phe^{13},Nle^{14}]-BN$^{6-14}$ by D-Tyr^6 produces only small differences in the adsorption mechanism of the resulting fragment (see Figure 5). These differences are due to the appearance of new bands (at 822 and 850 cm^{-1}) attributable to D-Tyr^6 ring vibrations, and these two weak bands do not change their enhancement as a function of Cu electrode potential (Figure 5C). On the other hand, their relative intensity on the Ag electrode at −1.200 V decreases with decreasing negative Ag electrode potential (Figure 5A). The reverse situation is observable on Au: here, at 0.400 V, the 823 cm^{-1} spectral feature reveals a pronounced enhancement (Figure 5B). The 1003 and 1602 cm^{-1} SERS signals are also quite strong in this spectrum, and they slightly decrease when the Au electrode potential becomes less negative. In contrast, the relative intensity of these two bands increases with increasingly negative electrode potential for [D-Tyr^6,β-Ala^{11},Phe^{13},Nle^{14}]BN$^{6-14}$ adsorbed on the Ag electrode. During this potential variation, the 1377 and 1606 cm^{-1} (see Table 1 for band assignment) SERS signals also gain intensity. However, none of the aforementioned bands change intensity as a function of potential in the SERS spectra of [D-Tyr^6,β-Ala^{11},Phe^{13},Nle^{14}]BN$^{6-14}$ deposited onto the Cu electrode surface, except for one barely detectable intensity decrease in the 1003 cm^{-1} spectra feature. The relative intensity of high wavenumber band near 3061 cm^{-1} due to aromatic stretching vibration ν(═C—H) increases at more positive electrode potentials for Cu electrode. Because the intensity of Trp^8 and Phe^{13} bands at 758 and 1003 cm^{-1}, respectively, increases in the same direction, observed changes point to the increased amount of adsorbed peptide at more positive electrode potential. These observations are supported by G2D-correlation maps of [D-Tyr^6,β-Ala^{11},Phe^{13},Nle^{14}]BN$^{6-14}$ adsorbed on Ag (Figure 11A), Au (Figure 11B), and Cu (Figure 11C) electrode surfaces. These maps also give some additional information: (i) all of the observed intensities shift in the same direction; (ii) on Ag, variations in the band enhancement take place first at 1377 and 1608 cm^{-1} followed by changes at 757 and 823 cm^{-1}, and last by changes at 1003 cm^{-1}; and (iii) on Au, the relative intensity modification at 1002 cm^{-1} takes place earlier than those at 1602 and 823 cm^{-1}. On the basis of the above observations, it can be proposed that the D-Tyr^6, Trp^8, and Phe^{13} rings "stand up" on the Cu electrode surface and do not alter their orientation when the electrode potential is changed. On the other hand, along with the decrease of the Cu electrode negative charge, the D-Tyr^6 ring slightly rises toward the surface normal. This movement forces the Phe^{13} ring to adopt a more vertical orientation on Au at 0.400 V than that at −1.200 V. In the case of the Ag electrode surface, small reorientation of Trp^8 (the indole ring is slightly lying

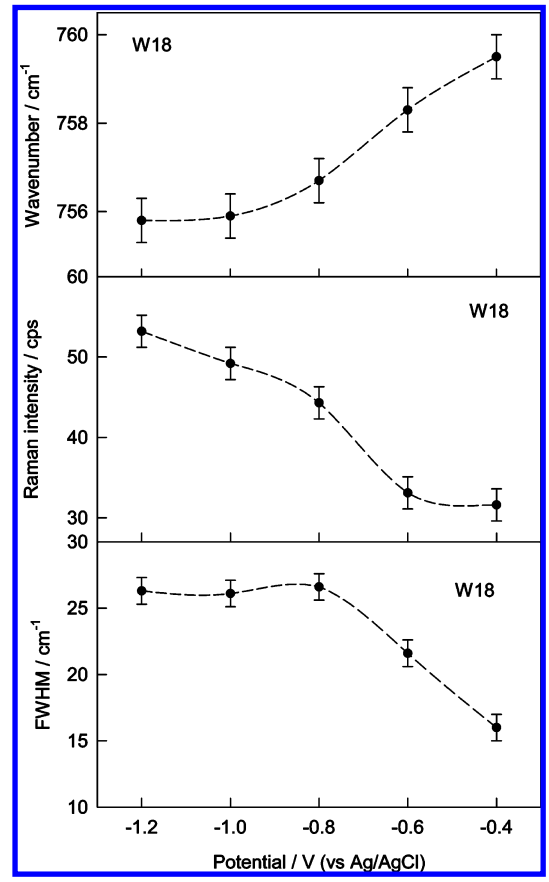

Figure 12. Dependence of W18 band position, intensity, and fwhm on the potential of a Cu electrode in 0.1 M Na_2SO_4 solution containing 0.01 M phosphate buffer (pH 7.0) and 10^{-5} M [D-Phe^6,β-Ala^{11},Phe^{13},Nle^{14}]BN$^{6-14}$.

down on Ag), when the electrode potential becomes less negative, initiates small differences in the interaction between D-Tyr^6 and Phe^{13} and the Ag surface.

Conclusions

Bombesin, like many biologically active peptides, is extremely difficult to detect by surface-enhanced Raman spectroscopy (SERS) because it has both a modest normal Raman cross section and it adsorbs weakly or not at all to metallic Ag, Au, and Cu surfaces. In this paper, we demonstrate a successful method for obtaining high-quality SERS spectra of specifically modified phenylalanine-substituted C-terminal 6−14 fragments (BN$^{6-14}$), which form amino acid sequences in bombesin: cyclo[D-Phe^6,His^7,Leu^{14}]BN$^{6-14}$, [D-Phe^6,Leu-NHEt^{13},des-Met^{14}]BN$^{6-14}$, [D-Phe^6,Leu^{13}-(Ⓡ)-p-Cl-Phe^{14}]BN$^{6-14}$, [D-Phe^6,β-Ala^{11},Phe^{13},Nle^{14}]BN$^{6-14}$, and [D-Tyr^6,β-Ala^{11},Phe^{13},Nle^{14}]BN$^{6-14}$. Also, we report for the first time a systematic potential-dependent and substrate-dependent study of interactions of these fragments with the roughened Ag, Au, and Cu electrode surfaces. This roughness can function as appropriate model systems for obtaining microscopic insights into the SERS enhancement mechanisms. Hence, the results reported here can be of importance for understanding the adsorption mechanism on the solid/liquid interface, elucidating the underlying mechanisms of the peptide−electrode surface interactions as a first step for the peptide−receptor problem. Also, understanding the conformation of these peptides on a given metal surface is fundamental for the research on the function of living systems. These experiments demonstrate the possibility of using SERS to investigate the interaction and kinetics of BN and its analogues and fragments with various molecules, a topic of high-priority interest in drug discovery and pharmaceutical development and testing. Thus, SERS is shown to be a useful technique for (1) elucidating peptide functionalities involved in bonding to roughened Ag, Au, and Cu electrode surfaces, (2) determining the peptide's molecular orientation with respect to these surfaces, (3) clarifying the peptide molecular conformation adopted on these surfaces, and (4) determining the substrate-dependent and potential-dependent changes in the peptide's molecular orientation.

Regardless of the composition and structure of these BN$^{6-14}$ fragments, the SERS spectra of our models exhibit similar adsorption mechanisms on Ag, Au, and Cu electrode surfaces at different applied potentials, almost identical spectral features dominated by Trp^8, Phe, and −CONH−. This indicates an interaction between Phe, Trp^8, and −CONH− and the roughened Ag, Au, and Cu electrode surfaces. On the basis of broadening and shift in wavenumbers of the Trp^8 W18 band, specific interaction of [D-Phe^6,Leu^{13}-(Ⓡ)-p-Cl-Phe^{14}]BN$^{6-14}$ and [D-Phe^6,β-Ala^{11},Phe^{13},Nle^{14}]BN$^{6-14}$ peptides with the Cu electrode surface at more negative potentials was suggested. Decrease of the Phe ring ν_{12} vibration wavenumber served as an indication of increased interaction of the aromatic moiety of [D-Phe^6,β-Ala^{11},Phe^{13},Nle^{14}]BN$^{6-14}$ with the Ag electrode surface at negative potentials. For other studied compounds, negligible bands shifting in wavenumber and bandwidth broadening do not point out direct interactions between these fragments and these metal substrates. However, small relative intensity variations of these SERS signals suggest some reorientation of these units on the metal substrates.

The observed SERS signals correlate well with the contribution of the structural components to the ability of these BN$^{6-14}$ fragments to interact with the rGRP-R. For example, the SERS patterns of five BN$^{6-14}$ fragments are similar and like that of full-length BN and its analogues,[40] suggesting that the first five amino acids of the BN N-terminus do not influence the adsorption mechanism on the roughened Ag, Au, and Cu electrodes similarly as they are not essential for interaction with the receptor.[21,22] Also, the SERS spectra of five BN$^{6-14}$ fragments, like those of BN, its modified analogues,[33,34,40] and related peptides,[35,36] mainly show the bands due to the Trp^8 residue. This may support a conclusion, drawn based on the biological activity studies, that Trp^8 is responsible for receptor recognition.[23] The enhancement of the Phe ring vibrations for BN$^{6-14}$ fragments may suggest that the side chains of the Trp^8 and Phe residues are oriented toward the same direction. Hence, it is more likely that these two residues interact with the metal surfaces.

Acknowledgment. This work was supported by the State Department for Scientific Research of the Ministry of Science and Higher Education (Grant No. N N204 159136 to E.P.). G.N. gratefully acknowledges the Department of Organic Chemistry at the Institute of Chemistry (Vilnius) for use of their Raman spectrometer.

References and Notes

(1) Plonowski, A.; Schally, A. V.; Varga, J. L.; Rekasi, Z.; Hebert, F.; Halmos, G.; Groot, K. *Prostate* **2000**, *44*, 172.
(2) Nock, B. A.; Nikolopoulou, A.; Galanis, A.; Cordopatis, P.; Waser, B.; Reubi, J. C.; Maina, T. *J. Med. Chem.* **2005**, *48*, 100.
(3) Santiskulvong, C.; Sinnett-Smith, J.; Rozengurt, E. *Am. J. Physiol. Cell Physiol.* **2001**, *281*, C886.
(4) Moody, T. W.; Chan, D.; Fahrenkrug, J.; Jensen, R. T. *Curr. Pharm. Des.* **2003**, *9*, 495.
(5) Qu, X.; Xiao, D.; Weber, H. C. *Curr. Opin. Endocrinol. Diabetes* **2003**, *10*, 60.
(6) Levine, L.; Lucci, J. A.; Pazdrak, B.; Cheng, J. Z.; Guo, Y. S.; Townsend, C. M.; Hellmich, M. R. *Cancer Res.* **2003**, *63*, 3495.
(7) Coy, D. H. Peptides, Chemistry and Biology, Proceedings of the 12th American Peptide Symposium, Cambridge, MA; Smith, J. A., Rivier, J. E., Eds.; Escom: Leiden, 1992; p 40.
(8) di Bello, C.; Gozzini, L.; Tonellato, M.; Corradini, M. G.; D'Auria, G.; Paolillo, L.; Trivellone, E. *FEBS Lett.* **1988**, *237*, 85.
(9) Mantey, S. A.; Coy, D. H.; Pradhan, T. K.; Igarashi, H.; Rizo, I. M.; Shen, L.; Hou, W.; Hocart, S. J.; Jensen, R. T. *J. Biol. Chem.* **2001**, *276*, 9219.
(10) Milusheva, E. A.; Milusheva, E. A.; Kortezova, N. I.; Mizhorkova, Z. N.; Papasova, M.; Coy, D. H.; Balint, A.; Vizi, E. S.; Varga, G. *Peptides* **1998**, *19*, 549.
(11) Thomas, F.; Arvelo, F.; Antoine, E.; Jacrot, M.; Poupon, M. F. *Cancer Res.* **1992**, *52*, 4872.
(12) Marion-Audibert, A. M.; Nejjari, M.; Pourreyron, C.; Anderson, W.; Gouysse, G.; Jacquier, M. F.; Dumortier, J.; Scoazec, J. Y. *Gastroenterol. Clin. Biol.* **2000**, *24*, 644.
(13) Rozengurt, E. *Trends Endocrinol. Metab.* **2002**, *13*, 128.
(14) Cullen, A.; Van Marter, L. J.; Allred, E. N.; Moore, M.; Parad, R. B.; Sunday, M. E. *Am. J. Respir. Crit. Care Med.* **2002**, *165*, 1093.
(15) Subramaniam, M.; Sugyiama, K.; Coy, D. H.; Kong, Y.; Miller, Y. E.; Weller, P. F.; Wada, K.; Wada, E.; Sunday, M. E. *Am. J. Respir. Crit. Care Med.* **2003**, *168*, 601.
(16) Xiao, D.; Chinnappan, D.; Pestell, R.; Albanese, Ch.; Weber, H. Ch. *Cancer Res.* **2005**, *65*, 9934.
(17) Xiao, D.; Qu, X.; Weber, H. C. *Cell Signal* **2003**, *15*, 945.
(18) Ganter, M. T.; Pittet, J. F. *Am. J. Respir. Crit. Care Med.* **2006**, *173*, 1.
(19) Bajo, A. M.; Schally, A. V.; Groot, K.; Szepeshazi, K. *Br. J. Cancer* **2004**, *90*, 245.
(20) Young, S. H.; Rozengurt, E. *Am. J. Physiol. Cell Physiol.* **2006**, *290*, C728.
(21) Moody, T. W.; Carney, D. N.; Cuttitta, P.; Quattrochi, K.; Gazdar, A. F.; Minna, J. D. *Life Sci.* **1985**, *37*, 105.
(22) Westendorf, J. M.; Schonbrunna, A. *J. Biol. Chem.* **1983**, *258*, 7527.
(23) Erspamer, V. *Comprehensive Endocrinology*; Glass, G. B. J., Ed.; John Wiley & Sons: New York, 1990; p 343.
(24) Coy, D. H.; Heinz-Erian, P.; Jiang, N. Y.; Sasaki, Y.; Taylor, J.; Moreau, J. P.; Wolfrey, W. T.; Gardner, J. D.; Jensen, R. T. *J. Biol. Chem.* **1988**, *263*, 5056.
(25) Nishino, H.; Tsunoda, Y.; Owyang, Ch. *Am. J. Physiol. Gastrointest. Liver Physiol.* **1998**, *274*, 525.

(26) Heimbrook, D. C.; Boyer, M. E.; Garsky, V. M.; Balishin, N. L.; Kiefer, D. L.; Oliff, A.; Riemen, N. W. *J. Biol. Chem.* **1988**, *263*, 7016.
(27) Saeed, Z. A.; Huang, S. C.; Coy, D. H.; Jiang, N. Y.; Heinz-Erian, P.; Mantley, S.; Gardner, J. D.; Jensen, R. T. *Peptides* **1989**, *10*, 597.
(28) Wang, L. H.; Coy, D. H.; Taylor, J. E.; Jiang, N. Y.; Kim, S. H.; Moreau, J. P.; Huang, S. Ch.; Mantey, S. A.; Frucht, H.; Jensen, R. T. *Biochemistry* **1990**, *29*, 616.
(29) United States Patent No. 5620959; Leban, J. J. (Kittsee, AT); Kull, F. C. (Durham, NC); Bombesin antagonists, 1997, Assignee Glaxo Wellcome Inc.
(30) Mantey, S. A.; Weber, H. Ch.; Sainz, E.; Akeson, M.; Ryan, R. R.; Pradhan, T. K.; Searles, R. P.; Spindel, E. R.; Battey, J. F.; Coy, D. H.; Jensen, R. T. *J. Biol. Chem.* **1997**, *272*, 26062.
(31) Podstawka, E.; Ozaki, Y.; Proniewicz, L. M. *Appl. Spectrosc.* **2004**, *58*, 1147.
(32) Podstawka, E.; Sikorska, E.; Proniewicz, L. M.; Lammek, B. *Biopolymers* **2006**, *83*, 193.
(33) Podstawka, E. *Biopolymers* **2008**, *89*, 506.
(34) Podstawka, E.; Ozaki, Y. *Biopolymers* **2008**, *89*, 807.
(35) Podstawka, E. *Biopolymers* **2008**, *89*, 980.
(36) Podstawka, E.; Proniewicz, L. M. *J. Phys. Chem. B* **2009**, *113*, 4978.
(37) Podstawka, E.; Ozaki, Y. *Biopolymers* **2008**, *89*, 941.
(38) Podstawka, E. *J. Raman Spectrosc.* **2008**, *39*, 1290.
(39) Podstawka, E.; Ozaki, Y.; Proniewicz, L. M. *Langmuir* **2008**, *24*, 10807.
(40) Podstawka, E.; Niaura, G. *J. Phys. Chem. B* **2009**, *113*, 10974.
(41) Aroca, R., Ed. *Surface-Enhanced Vibrational Spectroscopy*; Wiley: 2006.
(42) Niaura, G.; Gaigalas, A. K.; Vilker, V. L. *J. Raman Spectrosc.* **1997**, *28*, 1009.
(43) Bulovas, A.; Dirvianskytė, N.; Talaikytė, Z.; Niaura, G.; Valentukonytė, S.; Butkus, E.; Razumas, V. *J. Electroanal. Chem.* **2006**, *591*, 175.
(44) Kazakevičienė, B.; Valincius, G.; Niaura, G.; Talaikytė, Z.; Kažemėkaitė, M.; Razumas, V. *J. Phys. Chem. B* **2003**, *107*, 6661.
(45) Gao, P.; Gosztola, D.; Leung, L. W. H.; Weaver, M. J. *J. Electroanal. Chem.* **1987**, *233*, 211.
(46) Roth, E.; Hope, G. A.; Schweinsberg, D. P.; Kiefer, W.; Fredericks, P. M. *Appl. Spectrosc.* **1993**, *47*, 1794.
(47) Niaura, G.; Malinauskas, A. *Chem. Phys. Lett.* **1993**, *207*, 455.
(48) Niaura, G.; Gaigalas, A. K.; Vilker, V. L. *J. Phys. Chem. B* **1997**, *101*, 9250.
(49) Chalmers, J.; Griffiths, P. *Handbook of Vibrational Spectroscopy*; Wiley: Chichester, U.K., 2002.
(50) Dluhy, R.; Shanmukh, S.; Morita, S. I. *Surf. Interface Anal.* **2006**, *38*, 1481.
(51) Noda, I. *Appl. Spectrosc.* **1993**, *47*, 1329.
(52) Moskovits, M.; Suh, J. S. *J. Phys. Chem.* **1984**, *88*, 2931.

JP909268C